Lacticaseibacillus rhamnosus P118 enhances host tolerance to *Salmonella* infection by promoting microbe-derived indole metabolites

Baikui Wang[1,#], Xianqi Peng[2,3,#], Xiao Zhou[6], Xiuyan Jin[3], Abubakar Siddique[3], Jiayun Yao[2], Haiqi Zhang[2], Weifen Li[5], Yan Li[3,4], Min Yue[1,3,4,*]

1 Key Laboratory of Systems Health Science of Zhejiang Province, School of Life Science, Hangzhou Institute for Advanced Study, University of Chinese Academy of Sciences, Hangzhou 310024, China

2 Zhejiang Institute of Freshwater Fisheries, Ministry of Agriculture and Rural Affairs Key Laboratory of Healthy Freshwater Aquaculture, Key Laboratory of Fish Health and Nutrition of Zhejiang Province, Key Laboratory of Fishery Environment and Aquatic Product Quality and Safety of Huzhou City, Huzhou 313001, China

3 Department of Veterinary Medicine, Zhejiang University College of Animal Sciences, Hangzhou 310058, China

4 Hainan Institute of Zhejiang University, Sanya 572025, China

5 Institute of Animal Nutrition and Feed Sciences, Zhejiang University College of Animal Sciences, Hangzhou 310058, China

6. Ningbo Academy of Agricultural Sciences, Ningbo 315040, China

ORCID: Min Yue, https://orcid.org/0000-0002-6787-0794; Baikui Wang, https://orcid.org/0000-0001-5283-7337; Xianqi Peng, https://orcid.org/0000-0001-7143-8307

*** Corresponding Author: Professor Min Yue** (myue@zju.edu.cn)

[#] Baikui Wang and Xianqi Peng contributed equally to this work.

Abstract

Salmonella is one of the most common foodborne pathogens, resulting in inflammatory gastroenteritis and frequently accompanied by dysbiosis. Gut commensals, such as *Lactobacillus* species, have been proven to exhibit broad anti-bacterial activities and protect hosts against pathogenic infections. Here, *Lacticaseibacillus rhamnosus* strain P118, screened from 290 isolates recovered from fermented yoghurts and healthy piglet intestines using traditional and *C. elegans*-infection screening strategies, exerts great probiotic properties. Notably, P118 and its supernatant exhibited great antibacterial activities and attenuated *Caenorhabditis elegans* susceptibility to *Salmonella* infection. We found that P118 protected mice against *Salmonella* lethal infections by enhancing colonization resistance, reducing pathogen invasion, alleviating intestinal pro-inflammatory response, and improving microbial dysbiosis and fecal metabolite changes. Microbiota and fecal metabolome analyses suggested P118 administration significantly decreased the relative abundances of potentially harmful microbes (e.g., *Salmonella*, *Anaeroplasma*, *Klebsiella*) and increased the fecal levels of tryptophan and its derivatives (indole, indole-3-acrylic acid, 5-hydroxytryptophan, 5-methoxyindoleacetate). Deterministic processes determined the gut microbial community assembly of P118-pretreated mice. Integrated omics further demonstrated that P118 probiotic activities in enhancing host tolerance to *Salmonella* infection were mediated by microbe-derived tryptophan/indole metabolites (e.g., indole-3-acrylic acid, indole, tryptophan, 5-methoxyindoleacetic acid, and 5-hydroxytryptophan). Collective results demonstrate that *L. rhamnosus* P118 could enhance host tolerance to *Salmonella*

infections via various pathways, including direct antibacterial actions, inhibiting *Salmonella* colonization and invasion, attenuating pro-inflammatory responses of intestinal macrophages, and modulating gut microbiota mediated by microbe-derived indole metabolites.

Keywords: *Lacticaseibacillus rhamnosus*; *Salmonella* infection; intestinal dysbacteriosis; tryptophan metabolism; indole-3 acrylic acid; pro-inflammatory response

Introduction

Diarrhoeal diseases caused by infectious agents (e.g., pathogens and parasites) remain a severe health burden worldwide. Approximately 1.7 billion childhood diarrhoea cases are recorded annually, with diarrhea responsible for over 480 thousand deaths for children aged <5 years and over 500 thousand deaths for adults aged >70 years each year (Thiagarajah et al., 2015; UNICEF, 2022; WHO, 2017). As one of the most common foodborne enteric pathogens, *Salmonella* infection leads to substantial gastroenteritis incidents, imposing enormous economic burdens on global society and posing disproportionate threats to animal and human health (Kim and Isaacson, 2017; Stanaway et al., 2019). *Salmonella* has evolved strategies to subvert colonization resistance conferred by intestinal commensals and evade host immune defense responses, contributing to the increasing incidence of Salmonellosis (Caballero-Flores et al., 2022; Fu et al., 2019). *Salmonella*-contaminated food (meat, eggs, dairy) is considered the leading cause of Salmonellosis, estimated to cause a total global

67 economic loss of over $3.5 billion annually in the US (Kim and Isaacson, 2017).
68 Traditionally, antibiotic treatment has been the primary strategy to control *Salmonella*
69 infectious diseases (Eng et al., 2015). However, the global abuse of antibiotics has
70 raised significant concerns about antimicrobial resistance (AMR), foodborne antibiotic
71 residues, and compromises in treating antimicrobial resistant bacterial infections
72 (Fishbein et al., 2023; Olesen et al., 2018). These issues have inspired interest in seeking
73 alternative strategies, such as dietary interventions (e.g., probiotics, prebiotics, natural
74 products), to prevent *Salmonella* infectious disease outbreaks.
75 Microbial dysbiosis induced by antimicrobials, enteric infections, and irregular dietary
76 habits increases the susceptibility to pathogen infection and other diseases, such as
77 inflammatory bowel disease (Gillis et al., 2018b; Levy et al., 2017). Therefore, a
78 balanced intestinal microbiota and metabolic functions are crucial for maintaining
79 gastrointestinal homeostasis. Gut commensal microbes and their derivatives have been
80 proven to exhibit broad antimicrobial activities and protect the host against pathogen
81 infections by providing colonization resistance against enteric pathogens, limiting
82 pathogen colonization, invasion and transmission, and maintaining intestinal barrier
83 function (Caballero-Flores et al., 2023; Jacobson et al., 2018; Wan et al., 2019). As one
84 of the intestinal commensal microbes, probiotic species (without residues in raw food
85 products), such as *Lactobacillus*, *Bifidobacterium*, *Bacillus* and yeast (e.g.,
86 *Saccharomyces boulardii*, *S. cerevisiae*), exert beneficial effects on the host by
87 enhancing colonization resistance and immune defense, inhibiting colonization and
88 invasion against pathogens, and maintaining gastrointestinal homeostasis (Gareau et al.,

89 2010; Xiao et al., 2021). Although many candidate probiotic isolates have been
90 uncovered from fermented foods and mammalian intestines (Sakandar and Zhang, 2021;
91 Wang et al., 2022), the traditional strategies for screening these candidates are both
92 time-consuming and labor-intensive, involving bacterial isolation, culturing,
93 phenotypic characterization, randomized controlled trials, and various *in vitro* and *in*
94 *vivo* tests to assess probiotic properties (Sun et al., 2022). While culture-dependent
95 methods are classic strategies, emerging evaluation strategies for candidates, such as
96 whole-genome sequencing-based approaches and small invertebrate models (e.g., *C.*
97 *elegans*, *Drosophila*), have gained significant attention due to their high-throughput,
98 replicable and standardized properties (Sun et al., 2022; Wang et al., 2022).
99 Intestinal macrophages play vital roles in maintaining gut homeostasis, regulating
100 inflammation, and particularly in promoting the resolution of inflammation (Lavelle
101 and Sokol, 2020; Na et al., 2019), which has been considered as a novel potential target
102 for controlling intestinal pro-inflammatory disorders. It has been reported that
103 probiotics-derived metabolites, such as bacteriocins, antimicrobial compounds, short-
104 chain fatty acids, and tryptophan/indole derivatives, can mediate the beneficial effects
105 of probiotics on the host health by interacting with the host gastrointestinal immune
106 cells and gut residents (Britton and Faith, 2021; Sanders et al., 2019). Bacterial
107 tryptophan metabolism produces indole derivatives (e.g., indole-3-acetic acid, 3-
108 indolepropionic acid, 3-indoleacrylic acid, indole-3-lactic acid, indole-3-aldehyde,
109 indole-3-acetaldehyde), which are potent bioactive ligands for the aryl hydrocarbon
110 receptor (AHR) (Agus et al., 2018; Koh and Backhed, 2020). These indole derivatives

111 play crucial roles in maintaining gut barrier integrity and homeostasis by activating
112 AHR signaling pathway (Agus et al., 2018). *Limosilactobacillus reuteri*-produced
113 indole derivatives have been reported to exert anti-inflammatory effects by activating
114 AHR signaling pathway (Cervantes-Barragan et al., 2017). Although the beneficial
115 effects of probiotics in protecting the host against diverse enteric infections have been
116 extensively examined, the interactive roles between pro-inflammatory macrophages
117 and microbe-tryptophan/indole metabolites in combating enteric infections have not
118 been fully studied yet. Here, we found that *Lacticaseibacillus rhamnosus* P118 exerts
119 great probiotic properties after assessing by traditional and C. elegans-infection
120 screening strategies. P118 exhibited broad antibacterial activities and reduced host
121 susceptibility to enteric *Salmonella* infection by improving intestinal dysbiosis and
122 fecal metabolite changes, and inhibiting intestinal pro-inflammatory responses.
123 Integrated omics further demonstrated that P118 probiotic activities in enhancing host
124 tolerance to *Salmonella* infection were mediated by microbe-derived tryptophan/indole
125 metabolites.
126

127 **Results**

128 **Two screening approaches to convergent probiotic candidates**

129 A total of 290 bacterial isolates were isolated and identified from 33 fermented yoghurts
130 samples and 6 healthy piglet rectal content samples. Those isolates consist of 63
131 *Streptococcus* isolates, 158 *Lactobacillus/Lacticaseibacillus/Limosilactobacillus*
132 isolates, and 69 *Enterococcus* isolates (Figure 1A, Table 1). Two screening strategies

133 were employed in the present study to further investigate the potential probiotic
134 properties of the isolates: the traditional/classic approach and the *C. elegans* infection
135 approach. In the traditional/classic approach, 27 isolates were screened out by milk-
136 clotting activity assay (Figure 1A, Table S1), among which two isolates (P118 and P199)
137 exhibited the highest tolerance to bile salt (0.3%~2.0%) (Figure 1B) and biofilm
138 formation capabilities (Figure 1C). Compared with the P199 strain, P118 strain
139 exhibited the highest susceptibility to multiple antimicrobials (Figure S1A). *C. elegans*
140 has been widely used as an invaluable model for understanding the conserved
141 mechanisms of host-microbe interactions, due to the similarities of gut morphology and
142 physiological function with human and animal (Kumar et al., 2020). In the *C. elegans*
143 infection approach, 8 out of 290 isolates significantly increased the survivals and
144 prolonged the life span of *S*. Typhimurium-infected *C. elegans* ($P < 0.05$), and three
145 isolates (P118, P119, P120) treated worms were more resistant to *S*. Typhimurium
146 infection than the other isolates ($P < 0.05$) (Figure 1D, Table S2). Integrating the results
147 of both screening approaches, *L. rhamnosus* P118 strain exhibits versatile capabilities
148 as a probiotic candidate (Figure 1E).
149 To illustrate the probiotic properties of *L. rhamnosus* P118, antibacterial activity
150 evaluation *in vitro* was further conducted, and the results showed that the fermented
151 supernatants of P118 significantly inhibited the growth of multiple pathogens (e.g.,
152 *Salmonella*, *Yersinia*, *S. aureus*, *E. coli*, *C. rodentium*, *P. aeruginosa*, *R. anatipestifer*)
153 (Figure S1B). Interestingly, the inhibitory effect of P118 against *S*. Typhimurium was
154 in dose- and oxygen-dependent manners and results showed that high-dose and

155 anaerobic cultures exhibited more antibacterial effects than low-dose and aerobic
156 cultures, respectively ($P < 0.05$) (Figure 1F). Active factors derived from P118 to exert
157 antibacterial effects were explored. The results showed that the antibacterial activities
158 of the fermented supernatant (pH = 3.4) were sensitive to alkalinity (pH > 5.0), trypsin,
159 proteinase-K, pepsin and high temperature (> 70°C), but were resistant to catalase
160 treatment (Figure 1G-H). The fermented cultures and supernatants of P118 not only
161 significantly inhibited the growth of *S*. Typhimurium *in vitro* (Figure 1I), but also
162 protected worms against *S*. Typhimurium infection (Figure 1G, Table S3). Although
163 they exhibited no antibacterial activities *in vitro* (Figure 1I), the protective activities of
164 heat treated P118 and P118 lysates against *S*. Typhimurium pathogenesis were observed
165 in *C. elegans* but weaker than that of the fermented cultures and supernatants (Figure
166 1G).

167 **P118 genomics analysis suggests genetic determinants for antibacterial actions**

168 Subsequently, whole genome sequencing of P118 was performed to explore the
169 potential antibacterial factors based on genomic evidence. The results showed that
170 species-level identity for P118 isolate with 2.99 Mb genome size was confirmed at $P <$
171 0.0001 (Figure S2A, Figure 1K, Table S4), and P118 draft genome was most closely
172 related to *L. rhamnosus* subspecies (NCTC13710 and BIO5326) (Figure 1K, Table S5,
173 Figure S2B). Genomic analysis using antiSMASH and BAGEL4 databases revealed the
174 presence of putative bacteriocin synthesis genes in P118 isolate (Figure 1L). Putative
175 bacteriocins predicated in P118 isolate showed high homology with known class II
176 bacteriocins (IIa carnobacteriocin B2 produced by *C. maltaromaticum*, IIb enterocin X

177 produced by *Enterococcus faecium* KU-B5, IId/b lactococcin A/G, and some novel
178 bacteriocin-encoded hypothetical proteins). Collective data demonstrates that *L.*
179 *rhamnosus* P118 exhibits outstanding probiotic traits.

180 **P118 protects lethal *S*. Typhimurium infections in a murine model**

181 The protective activity of *L. rhamnosus* P118 against enteric pathogens was further
182 examined in the *Salmonella*-infected murine model (Figure 2A). Administration of
183 P118 significantly protected mice against *Salmonella*-induced deaths and body weight
184 losses (Figure 2B-C), accompanied by the alleviated splenomegaly, hepatomegaly,
185 shortened gastrointestinal tract and clinical and pathological score (Figure 2D-F, Figure
186 S3B). Meanwhile, P118 significantly limited *Salmonella* colonization in the intestinal
187 tissues (duodenum and colon) and invasion into the peripheral organs (liver and spleen)
188 of mice, thereby markedly reducing *Salmonella* fecal shedding (Figure 2G).
189 Additionally, *Salmonella* infection-induced ileal mucosal damage was alleviated by
190 P118 administration, as illustrated by the increased ileal villus height (Figure 2H, Figure
191 S3C), ratio of villus height/crypt-depth (Figure 2H, Figure S3D), ileal microvilli height
192 and density (Figure 2H, Figure S3E-F), the upregulated ZO-1 mRNA expression
193 (Figure S4A), and the downregulated *IL-1β* mRNA expression (Figure S4E),
194 accompanied by the reduced IL-1β level in serum (Figure S4D). Intervention with P118
195 significantly increased the numbers of Ki67-positive cells (proliferating cells), Muc2-
196 positive cells (goblet cells), and decreased the numbers of F4/80-positive cells
197 (macrophages) and F4/80^{+} iNOS^{+} cells (pro-inflammatory macrophages) in the ileum
198 (Figure 2H) and also attenuated the pathological damages of peripheral organs (liver

199 and spleen) caused by *Salmonella* infection (Figure S3A & B).

200 **P118 improves *Salmonella* infection by modulating gut microbiota**

201 Gut microbes play crucial roles in host physiological activities, and colonization
202 resistance against enteric pathogens (Jacobson et al., 2018), and dysbiosis is supposedly
203 associated with *Salmonella* infection (Gillis et al., 2018a). Significant bacterial
204 community structures among four groups were observed (Figure 3A, Table S8), and
205 most of the bacterial operational taxonomic units (OTUs) were classified as group-
206 specific OTUs (Figure 3B). Compared to the uninfected group, *Salmonella* infection
207 significantly depleted 167 OTUs and enriched 60 OTUs (Figure 3C), whereas
208 compared to the *Salmonella*-infected group, pretreatment with P118 significantly
209 depleted 16 OTUs and enriched 52 OTUs (Figure 3D). Specifically, *Salmonella*
210 infection significantly increased the relative abundances of potentially harmful
211 microbes (e.g., *Salmonella*, *Escherichia*-Shigella, *Klebsiella*, *Morganella*,
212 *Akkermansia*) and significantly reduced the relative abundances of SCFA-producing
213 and potentially beneficial microbes (e.g., *Alloprevotella*, *Lactococcus*,
214 *Faecalibacterium*, *Limosilactobacillus*, *Parasutterella*, *Odoribacter*, *Dubosiella*,
215 *Candidatus arthromitus*) (Figure 3E, Figure S5B). Pretreatment with P118 significantly
216 reduced the relative abundances of pathogenic microbes (e.g., *Salmonella*,
217 *Anaeroplasma*, *Klebsiella*, *Morganella*) and significantly increased the relative
218 abundances of potentially beneficial or commensal microbes (e.g.,
219 *Candidatus_Saccharimonas*, *Turicibacter*, *Enterorhabdus*) (Figure 3F, Figure S5C).
220 Based on the changes in bacterial community structures, the internal driving forces of

221 gut microbial communities were investigated using ecological models. Both null model
222 and neutral community model analyses revealed that the stochastic processes belonging
223 to homogenizing dispersal exerted important roles in *Salmonella*-infected mice gut
224 microbiome assembly, whereas the deterministic processes (homogeneous selection
225 and variable selection) exerted more influences on P118-pretreated mice gut
226 microbiome assembly than *Salmonella*-infected mice (Figure S6A-B).

227 **Microbe-derived tryptophan metabolites are associated with the protection**

228 Significant differences in fecal metabolite structures among the three groups separated
229 into distinct clusters were also observed (Figure 4A, Table S9). Compared with the
230 uninfected group, *Salmonella* infection significantly upregulated 256 fecal metabolites
231 ($\log_2$(fold change) > 1, $P < 0.05$) and downregulated 402 fecal metabolites ($\log_2$(fold
232 change) < 1, $P < 0.05$) (Figure 4B), and pretreatment with P118 significantly enriched
233 100 metabolites ($\log_2$(fold change) > 1, $P < 0.05$) and depleted 81 metabolites ($\log_2$(fold
234 change) < 1, $P < 0.05$) (Figure 4C). Among the significant differential metabolites, 91
235 metabolites (VIP > 1) downregulated in *Salmonella*-infected mice were upregulated
236 explicitly in P118-pretreated mice (Figure S7A&C, Table S10), and 43 metabolites
237 (VIP > 1) upregulated in *Salmonella*-infected mice were downregulated explicitly in
238 P118-pretreated mice (Figure S7B&C, Table S10). KEGG pathway analysis revealed
239 that fecal metabolites were mainly enriched in tryptophan metabolism, fatty acid
240 biosynthesis, biosynthesis of amino acids and neuroactive ligand-receptor interaction
241 pathways in P118-pretreated mice (Figure 4D). Interestingly, pretreatment with P118
242 significantly increased the fecal levels of tryptophan and tryptophan derivatives (indole,

243 indole-3-acrylic acid, 5-hydroxytryptophan, 5-methoxyindoleacetate) (Figure 4E).
244 Pearson correlation analysis showed that *S.* Typhimurium burdens (in the duodenum,
245 colon, liver, spleen, feces) and organ (spleen, liver) indices were negatively correlated
246 with the levels of fecal tryptophan and tryptophan derivatives (indole, indole-3-acrylic
247 acid, 5-hydroxytryptophan, protocatechuic acid, trans-cinnamaldehyde, 5-
248 methoxyindole-3-carbaldehyde) and positively correlated with the levels of (serotonin,
249 tryptophanol, 3-(2-hydroxyethyl) indole, tryptamine) (Figure 4F). Conversely, the body
250 weight was positively correlated with the levels of fecal tryptophan and tryptophan
251 derivatives (Figure 4F). Bio-Sankey network analysis further showed that 26 genera
252 were identified as potential bacteria that might participate in the metabolic reaction
253 R02340 (tryptophan synthase, indoleglycerol phosphate and indole), of which five
254 bacteria (*Bifidobacterium*, *Lacticaseibacillus*, *Enterococcus*, *Staphylococcus*, and
255 *Pseudomonas*, dark red if $P < 0.05$) were positively associated with indole in the
256 metabolic reaction R02340 (Figure 4G). These results indicate that microbe-derived
257 tryptophan metabolites are associated with P118-mediated protection against
258 *Salmonella* infection.
259 Based on the findings above that *Lacticaseibacillus* species were involved in
260 tryptophan biosynthesis and metabolism, *L. rhamnosus* P118 genome was reanalyzed
261 to determine whether P118 encode enzymes necessary to exert this function. The
262 genomic data further showed that P118 encoded various genes (e.g., *fldH*, *AraT*, *AspB-*
263 *4*, *AmiE*, *trpA*, *trpB*, *BCAT*, *IGPS*, *MT*) essential to biosynthesize and metabolize
264 tryptophan into tryptophan derivatives (Figure 4H, Table S11). The metabolomic results

265 of P118 cultures also validated the genomic data that P118 could secrete a diverse
266 profile of tryptophan-derived metabolites (e.g indole-3-acrylic acid, indole, indole-3-
267 lactic acid, DL-tryptophan, kynurenine, N-Acetyl-D-tryptophan, 5-
268 methoxyindoleacetic acid, 5-hydroxytryptophan) (Table S12). Taken together, these
269 data suggest that P118-derived tryptophan metabolites might contribute to the
270 protection against *Salmonella* infection.

271 **Indole-3-acrylic acid protects against *Salmonella* infection by inhibiting**
272 **macrophage pro-inflammatory responses**

273 Based on the above results, exogenous indole-3-acrylic acid (IAA) was employed to
274 further explore its roles against *Salmonella* infection. The antibacterial assay results
275 showed that IAA (> 4.4 mM) significantly inhibited *Salmonella* growth (Figure S8).
276 Exogenous IAA administration significantly reduced mice susceptibility to *Salmonella*
277 infection， as evidenced by the increased body weight (Figure 5B), the alleviated
278 splenomegaly and hepatomegaly (Figure 5D, 5F), and the increased colon length
279 (Figure 5C). Meanwhile, IAA administration significantly inhibited *Salmonella*
280 colonization in the intestinal tissues (cecum and colon) and invasion into the peripheral
281 organs (liver and spleen) of mice, thereby markedly reducing *Salmonella* fecal shedding
282 (Figure 5E). Additionally, *Salmonella* infection-induced ileal mucosa damage was
283 alleviated by exogenous IAA, as illustrated by the increased ileal villus height (Figure
284 5G, 5I), and the increased numbers of Muc2-positive goblet cells in the ileum (Figure
285 5H, 5I). Exogenous IAA intervention significantly reduced *Salmonella* infection-
286 induced intestinal pro-inflammatory responses, as evidenced by the decreased numbers

287 of F4/80-positive macrophages (Figure 5I), the downregulated mRNA (*IL-1β*, *IL-6*, *IL-*
288 *18*, *TNF-α*, *iNOS*) expression (Figure 5H), and the reduced protein (iNOS, IL-1β, IL-6,
289 TNF-α, markers of pro-inflammatory macrophages) expression (Figure 5I).
290 The *in vitro* experiments further showed that, although failed to increase the uptake of
291 *Salmonella* (Figure S9A, 0h), IAA treatment significantly reduced intracellular
292 *Salmonella* survival in RAW 264.7 macrophage cells (Figure S9A, 6h, 12h), which
293 could be reversed by pretreatment with AHR inhibitor CH-223191 (Figure S9A, 6h,
294 12h), indicating that IAA enhances the intracellular bactericidal capacity of RAW 264.7
295 cells. Furthermore, IAA treatment significantly inhibited *Salmonella* infection-induced
296 pro-inflammatory responses, as evidenced by inhibiting mRNA (*IL-1β*, *IL-6*, *IL-18*,
297 *TNF-α*, *iNOS*) expression and nitric oxide secretion of *Salmonella*-infected RAW 264.7
298 macrophage cells, which blocked by the presence of AHR inhibitor CH-223191 (Figure
299 S9B-G).
300 Macrophages play important roles in initiating immune responses, maintaining gut
301 homeostasis and phagocytic clearance of pathogens (Na et al., 2019). To further
302 investigate the involved roles of macrophages in P118/IAA-mediated protective effect,
303 *in vivo* macrophage depletion using clodronate liposomes was conducted. As expected,
304 macrophage depletion significantly blocked the protection of P118 and exogenous IAA
305 against *Salmonella* infection (Figure 6A-I). P118 or exogenous IAA administration
306 failed to increase the body weight (Figure 6B) and colon length (Figure 6E), alleviate
307 the splenomegaly and hepatomegaly (Figure 6C, 6D), inhibit the colonization, invasion
308 and shedding of *Salmonella* (Figure 6F) after the intestinal macrophage depletion.

309 Additionally, after depleting the intestinal macrophage, P118 or exogenous IAA
310 administration also failed to attenuate *Salmonella* infection-induced intestinal mucosa
311 damage (Figure 6G, 6H, 6I) and pro-inflammatory responses (Figure 6H, 6I). Taken
312 together, these findings indicate that P118 and IAA protect against *Salmonella* infection
313 by inhibiting pro-inflammatory responses of intestinal macrophage.
314

315 **Discussion**

316 Fermented foods and mammalian intestines are rich in lactic acid bacteria that can
317 produce organic acids and lactobacillin to inhibit overgrowth, adhesion, invasion and
318 toxin secretion of pathogens (Gareau et al., 2010; Wan et al., 2019). Traditionally, the
319 culturomics strategy, together with multiple evaluation assays, is the primary way to
320 search potential probiotic species from the complex microbial community, which is
321 both time- and labor-consuming (Wang et al., 2022). Although the whole genomic
322 sequencing-based approach is an emerging favorable way to screen potential probiotic
323 strains, it's hard to widely adopt based on numerous isolates due to the high sequencing
324 costs (Schwarze et al., 2020). Given that the similarities of gut morphology and
325 physiological function with human and animal, *C. elegans* provides an invaluable
326 model to investigate host-microbe interactions and probiotic properties of beneficial
327 microbes at low cost (Kumar et al., 2020; Poupet et al., 2020). In the present study, we
328 found *Salmonella* infection significantly induced death and decreased the lifespan of *C.*
329 *elegans*, indicating *C. elegans* is very susceptible to *S.* Typhimurium infection,
330 consistent with a previous report (Rangan et al., 2016). Integrating the results of

331 culturomics and *C. elegans* infection strategies, *L. rhamnosus* P118 with excellent
332 probiotic properties was screened from 290 isolates and exhibited broad *in vitro*
333 antibacterial activities. Interestingly, high fermented dose and anaerobic cultures of
334 P118 showed more antibacterial effects than low dose and aerobic cultures, indicating
335 that the active factors were more released by P118 at the stationary phase under
336 anaerobic conditions. What's more, the antibacterial activities of the fermented
337 supernatant were sensitive to alkalinity, trypsin, proteinase-K, pepsin, and high
338 temperature, indicating that the active secreted factors in the fermented supernatant
339 were protein- or peptide-based active agents, consistent with a previous report that *L.*
340 *rhamnosus* exerted antibacterial effects by secreting bioactive peptides (Iram et al.,
341 2022). Although limited studies have reported bacteriocin-like activity in *L. rhamnosus*,
342 it remains unclear whether this species produces active bacteriocins (Kankainen et al.,
343 2009). Nonetheless, genomic data in this study revealed the presence of putative
344 bacteriocin synthesis genes in P118 genome. In agreement with a previous study
345 (Kankainen et al., 2009), the predicated bacteriocins showed high homology with
346 known class II bacteriocins (e.g., IIa carnobacteriocin B2 produced by *C.*
347 *maltaromaticum*, IIb enterocin X produced by *Enterococcus faecium* KU-B5), which
348 needs to be further validated by gene-editing technology and synthetic biology.
349
350 To further validate the antibacterial activities of *L. rhamnosus* P118 against enteric
351 pathogens, *Salmonella*-infected mice model was employed. We found that
352 administration of P118 significantly reduced mice susceptibility to *S.* Typhimurium

353 infection by improving intestinal health, dysbiosis and the changes of fecal metabolite
354 profiles. Colonized *S.* Typhimurium in the intestine disrupts structural and functional
355 intestinal integrity, leading to substantial immune response and severe epithelial barrier
356 damage, and then migrates to internal organs (liver, spleen) via the blood circulatory
357 system, causing splenomegaly and hepatomegaly (Rogers et al., 2022; Wang et al.,
358 2021a). In the present study, P118 significantly increased *Salmonella*-infected mice
359 survival and alleviated *Salmonella*-induced splenomegaly and hepatomegaly. The
360 beneficial attenuated effect was partly contributed by the reduced *Salmonella*
361 colonization in intestine and invasion into the peripheral organs, and eventually, the
362 decreased fecal shedding, consistent with previous reports (Liu et al., 2023; Wu et al.,
363 2024). It's reported that *S.* Typhimurium exploits and disrupts intestinal barrier integrity
364 to adhere, and disseminate deeper into intestinal mucosa, and evade immune clearance
365 (Bernal-Bayard and Ramos-Morales, 2018; Hiyoshi et al., 2022). In the current study,
366 P118 treatment also significantly improved the structural and functional intestinal
367 integrity, attenuated inflammatory responses, reduced the numbers of F4/80-positive
368 macrophages and proinflammatory macrophages ($F4/80^+$ $iNOS^+$ cells), and increased
369 the numbers of Ki67-positive and Muc2-positive goblet cell in the ileum, demonstrating
370 that P118 improved the intestinal health and reducing pro-inflammatory responses of
371 intestinal macrophages, which further confirms the beneficial alleviated effect exerted
372 by *L. rhamnosus* P118.
373
374 Intestinal microbes play essential roles in providing colonization resistance against

375 enteric pathogens and pathobionts, and limiting adhesion, invasion and transmission of
376 pathogens (Caballero-Flores et al., 2022; Jacobson et al., 2018). Microbial dysbiosis
377 and excessive immune responses induced by enteric pathogens can, in turn, aggravate
378 and exacerbate gut permeability and damage (Read et al., 2021; Rogers et al., 2022).
379 Many studies have reported that *Salmonella* infection was often accompanied by
380 microbial dysbiosis (Gillis et al., 2018b; Read et al., 2021; Wang et al., 2021a). The
381 current results found that *L. rhamnosus* P118 treatment significantly restored the
382 bacterial community structures in *Salmonella*-infected mice, and significantly reduced
383 the relative abundances of potentially harmful microbes (e.g., *Salmonella*, *Klebsiella*,
384 *Anaeroplasma*, *Morganella*), which belong to pathogens and pathobionts (Dong et al.,
385 2022; Galan, 2021; Laupland et al., 2022). Structure composition and assembly of
386 microbial communities are essential for ecosystem function (Shi et al., 2023; Xun et al.,
387 2019), and revealing the underlying mechanisms of microbial community assembly is
388 a major goal of microbial community ecology (Jiao et al., 2020; Stegen et al., 2012).
389 Generally, stochastic (e.g., dispersal events, ecological drift, random birth, death) and
390 deterministic (e.g., interspecies interactions (e.g., competition, facilitation, mutualisms
391 and predation), species traits, environmental factors) processes are two major
392 ecological processes that drive microbiome assembly (Stegen et al., 2012; Zhou and
393 Ning, 2017). Deterministic processes mainly involve non-random and niche-based
394 mechanisms with abiotic and biotic factors that influence microbial community
395 assembly (Vellend, 2010), whereas stochastic processes mainly reflect random changes
396 in the relative abundance of species (Jiao et al., 2020; Jiao et al., 2021). Although

397 important in shaping the diversities of microbial composition and functions, the relative
398 contribution of microbiome assembly processes varies with different habitats (Jiao et
399 al., 2020; Jiao et al., 2021). The present study revealed that the stochastic processes
400 played dominant roles in intestinal microbiome assembly in *Salmonella*-infected mice,
401 indicating random changes occurred in the relative abundance of species. Conversely,
402 the deterministic processes played more significant roles in driving intestinal microbial
403 community assembly in P118-pretreated mice than in *Salmonella*-infected mice,
404 indicating abiotic factors (e.g., dietary intervention) or biotic interactions (e.g.,
405 microbial competition, facilitation, mutualism, predation, host filtering) might
406 influence the microbial community.
407
408 Accumulating evidence revealed that gut microbes-derived metabolites (e.g., short-
409 chain fatty acids, tryptophan/indole-derived metabolites, bacteriocins, bile acid, natural
410 products) are crucial mediators in host physiological activities (Cani, 2019; Wlodarska
411 et al., 2017), and metabolic disorders are major risk factors for bacterial infections
412 (Olive and Sassetti, 2016). In this study, the results showed that *L. rhamnosus* P118
413 improved *Salmonella* infection-induced fecal metabolite changes. Interestingly, P118
414 significantly increased the fecal levels of tryptophan and its derivatives (indole, indole-
415 3-acrylic acid, 5-hydroxytryptophan), and those metabolites were negatively correlated
416 with *S.* Typhimurium burdens (in the duodenum, colon, liver, spleen, feces) and organ
417 (spleen, liver) indices, and positively correlated with the body weight of mice,
418 indicating that microbiota-derived tryptophan/indole metabolites play beneficial roles

419 in P118 mediated probiotic activities in enhancing host tolerance to *Salmonella*
420 infection. It's reported that through binding to the aryl hydrocarbon receptor (AHR) of
421 host, bacterial tryptophan derivatives act as triggers to stimulate immune responses and
422 gut hormones to exert anti-inflammatory activities, enhance intestinal epithelial barrier,
423 and promote gastrointestinal motility, which contributes to host gastrointestinal
424 homeostasis and health (Agus et al., 2018; Cani, 2019). Our genomic and metabolomic
425 data further revealed that P118 could produce a wide array of tryptophan-derived
426 metabolites owing to encoding a variety of enzyme genes necessary to metabolize
427 tryptophan into indole derivatives; consistently, some *Lactobacillus* species broadly
428 conserved enzyme encoding genes that are involved in tryptophan metabolism
429 (Montgomery et al., 2022). The above results indicate that *L. rhamnosus* P118- and
430 microbe-derived tryptophan/indole metabolites might play positive roles in P118-
431 mediated probiotic activities. Although significant increases in microbe-derived
432 tryptophan/indole metabolites were observed in P118-treated mice, and it was
433 established that P118 can metabolize tryptophan into indole derivatives, it remains to
434 be investigated whether the differential tryptophan/indole metabolites were directly
435 derived from P118 or from other microbes. To test the roles of differential
436 tryptophan/indole metabolites in P118-mediated beneficial effects, exogenous indole-
437 3-acrylic acid, which significantly and negatively correlated with *S.* Typhimurium
438 burdens and hepatosplenomegaly mentioned above, was employed to investigate its
439 protective effect against *Salmonella* infection. Interestingly, we found that indole-3-
440 acrylic acid administration significantly enhanced mice tolerance to *S.* Typhimurium

441 infection by improving intestinal health and attenuating pro-inflammatory responses of
442 intestinal macrophages. Furthermore, the *in vitro* results also provide that indole-3-
443 acrylic acid enhanced bactericidal capacity of RAW 264.7 cells and inhibited *S.*
444 Typhimurium-induced pro-inflammatory responses, consistent with a previous report
445 (Wlodarska et al., 2017). Taken together, these results demonstrate that *L. rhamnosus*
446 P118/microbe-derived indole-3-acrylic acid play beneficial roles in P118-mediated
447 probiotic activities.
448 Macrophages are important in initiating immune responses, maintaining intestinal
449 immune homeostasis, phagocytic clearance of pathogens, tissue repair, and host defense
450 (Na et al., 2019; Neurath, 2024). It's reported that macrophages with strong plasticity
451 could be polarized into pro-inflammatory (M1) phenotype or proresolving (M2)
452 phenotype (Na et al., 2019). M1 macrophage activation is crucial and necessary for
453 pathogen clearance (Na et al., 2019). However, exaggerated immune responses
454 triggered by M1 macrophage are detrimental to the host by inducing tissue damage and
455 cell deaths (Wang et al., 2020). The current study showed that both *L. rhamnosus* P118
456 and indole-3-acrylic acid significantly attenuated *S.* Typhimurium infection-induced
457 pro-inflammatory responses, indicating that pro-inflammatory macrophages might be
458 key targets for *L. rhamnosus* P118 exerting probiotic effect. This hypothesis was
459 confirmed by macrophage depletion experiments that the protective effects of *L.*
460 *rhamnosus* P118 and indole-3-acrylic acid against *Salmonella* infection were abrogated
461 after intestinal macrophage depletion. Taken together, these results indicate that *L.*
462 *rhamnosus* P118/microbe-derived indole metabolites enhance host tolerance to

463 *Salmonella* infection by reducing intestinal pro-inflammatory responses, which also
464 provides a potential alternative strategy for using probiotics and their derived
465 metabolites to treat intestinal inflammatory disorders such as inflammatory bowel
466 disease (Lavelle and Sokol, 2020; Neurath, 2024).

467 **Conclusion**

468 In summary, two distinctive approaches were used to screen the probiotic candidate,
469 and the P118 strain was underscored for beneficial effects on a murine infection model.
470 Further, bacterial genomic sequencing, gut microbiota and metabolomic analysis
471 pinpointed the microbe-derived tryptophan/indole could be the importance of P118
472 probiotic properties. Nevertheless, the newly found P118 could enhance host tolerance
473 to *Salmonella* infections via various pathways, including direct antibacterial actions,
474 inhibiting *Salmonella* colonization and invasion, attenuating pro-inflammatory
475 responses of intestinal macrophages, and modulating gut microbiota mediated by
476 microbe-derived indole metabolites (Figure 7).

477

478 **Materials and methods**

479 **Bacterial isolation and culture**

480 Lactic acid bacteria (LAB) and *Enterococcus* strains were isolated from 39 samples: 33
481 fermented yoghurts samples (collected from families in multiple cities of China,
482 including Lanzhou, Urumqi, Guangzhou, Shenzhen, Shanghai, Hohhot, Nanjing,
483 Yangling, Dali, Zhengzhou, Shangqiu, Harbin, Kunming, Puer), and 6 healthy piglet
484 rectal content samples without pathogen infection and diarrhea in pig farm of Zhejiang

485 province. De Man-Rogosa-Sharpe (MRS) with 2.0% CaCO3 and Brain heart infusion
486 (BHI) broths (Huankai Microbial, Guangzhou, China) were used for bacteria isolation.
487 Matrix-Assisted Laser Desorption Ionization-Time of Flight Mass Spectrometry
488 (MALDI-TOF MS, Bruker Daltonik GmbH, Bremen, Germany) method was employed
489 to identify of bacterial species with a confidence level ⩾ 90% (He et al., 2022).
490 *Lacticaseibacillus rhamnosus* P118 (P118) and *Salmonella enterica* serovar
491 Typhimurium SL1344 (STm) were cultured in MRS and Luria Broth (LB) medium at
492 37 °C overnight under aerobic conditions, separately. The final concentration of
493 bacterial isolates was constantly checked by the spreading plate method (Wang et al.,
494 2023). After being centrifugated at 4000× g for 15 min at 4 °C, the fermented
495 supernatant of *L. rhamnosus* P118 was collected by centrifugation at 4000× g for 15
496 min at 4 °C, and then filtered through a 0.22 μm membrane (Merck Millipore,
497 Burlington, MA, USA) kept at 4 °C for further use.

498 **Probiotic property evaluation of candidate isolates**

499 For milk-clotting activity analysis of probiotics (Zhang et al., 2023), overnight
500 fermented lactic acid bacteria isolates under logarithmic growth were added to test
501 tubes containing skim milk (10% skim milk with 10 mM $CaCl_2$) at 1:20 ratio (v/v) and
502 then incubated at 37 °C. The coagulating time, final pH value and acidity of milk were
503 measured during the curdling process.

504 The bile salt tolerance assay was conducted according to a previous report (Wang et al.,
505 2023). Briefly, the isolates under logarithmic growth were resuspended into fresh MRS
506 medium (1% v/v) containing different (wt/v, 0, 0.3%, 0.6%, 1.0%, 1.5%, 2.0%) porcine

507 bile (MACKLIN®, Shanghai, China) and then plated into 96-well plates, after
508 incubation for 24h at 37 °C, the absorbance at 620 nm was measured by a SpectraMax
509 M5 reader (Molecular Devices, Sunnyvale, CA, USA).
510 Biofilm-forming assay of the isolates was performed as described previously (Zhou et
511 al., 2023). Briefly, 200 μL overnight cultures (adjusted to 2×10^6 CFU/mL) were added
512 into 96-well flat-bottom plates. After incubation for 36h at 37 °C, the planktonic cells
513 were discarded. After being gently washed three times with sterile PBS, the adherent
514 cells were stained with 200 μL of 0.4% crystal violet for 15 min at room temperature
515 and then washed with sterile PBS three times again. Finally, 200 μL 75% ethanol was
516 added to dissolve the stained adherent cells for 15 min, and biofilm was quantified by
517 measuring the absorbance at 590 nm using a SpectraMax M5 reader.
518 For antimicrobial susceptibility test, twelve antimicrobial agents (penicillins (PG),
519 erythromycin (EM), lincomycin (LM), gentamicin (GM), doxycycline (DOX),
520 ceftriaxone (CTR), norfloxacin (NOR), azithromycin (AZM), fleroxacin (FLE),
521 vancomycin (VA), streptomycin (STR)) were employed to evaluate the antimicrobial
522 susceptibility of the candidate probiotics by utilizing the Kirby-Bauer disk diffusion
523 method (Hudzicki, 2009).
524 The agar diffusion method (Wang et al., 2023) was used to evaluate the antimicrobial
525 activity against multiple pathogens *in vitro*. Briefly, bacterial culture medium (LB, BHI)
526 containing 0.25% (v/v) different zoonotic pathogens under logarithmic growth was
527 poured into 10-cm plates (Corning, NY, USA), separately. Then, 200 μL of the
528 fermented sterile supernatant collected from the overnight cultured *L. rhamnosus* P118

529 was added into 8 mm agar wells created by Oxford cup. The bacteriostatic effect was
530 evaluated by the growth inhibition zone around the 8-mm agar wells after overnight
531 incubation at 37 °C.

532 ***Caenorhabditis elegans* infection**

533 *C. elegans* infection model was performed as previously described (Rangan et al., 2016).
534 *C. elegans* N2 (Bristol) were routinely raised on Nematode Growth Media (NGM)
535 feeding with *E. coli* OP50, and L4-stage worms were prepared according to the
536 description in WormBook (Girard et al., 2007). 200 μL of the isolated isolates (adjusted
537 to 5×10^8 CFU/mL using M9 medium) and *L. rhamnosus* P118-related substances (e.g.,
538 mixed cultures, fermented sterile supernatants, P118 lysate, dead P118) were poured
539 onto NGM in 24-well plates, separately, and dried at 22 °C for 4 h. L4-stage worms
540 were then transferred to the lawns of the poured NGM plates (30 worms/plate) with
541 three plates per group for 24h. Then, the treated worms were washed and transferred to
542 lawns of STm (1×10^8 CFU/lawn) on NGM plates for infection. Worm survival was
543 monitored at 24-hour intervals for sixteen days.

544 **Whole genome sequencing and data analysis**

545 Whole genome sequencing, quality control, assembly and annotation of *L. rhamnosus*
546 P118 was conducted according to our previous study (Zhou et al., 2023) using PacBio
547 Sequel platform and Illumina NovaSeq PE150 at Novogene (Novogene Co, Ltd.,
548 Beijing, China), and the P118 draft genome is available in the Sequence Read Archive
549 under accession number PRJNA848987. *L. rhamnosus* P118 assembly was queried
550 against the NCBI non-redundant prokaryotic genomes database using the Microbial

551 Genomes Atlas (MIGA) webserver (database update to 10/10/2023) (Rodriguez et al.,
552 2018). Taxonomic classification was inferred by the maximum average amino acid
553 identity (AAI) against all genomes in the database, with p-values estimated from the
554 distribution of all the reference genomes in NCBI's RefSeq at each taxonomic level as
555 a readout of classification probability. Average nucleotide identity (ANI) and AAI
556 tables of maximally the top-50 reference hits in the database were extracted and graphed
557 as x-y scatter plots to determine the nearest phylogenetic neighbors. To generate
558 phylogenic trees of isolates and MIGA-identified nearest phylogenetic neighbors, the
559 interfered proteome from PROKKA isolate annotations, or as publicly available in
560 NCBI for applicable reference genomes were uploaded to the ANI/AAI-Matrix
561 calculator (Rodriguez-R and Konstantinidis, 2016). The resulting phylogenetic tree
562 based on AAI was visualized using the interactive tree of life (iTOL) (Letunic and Bork,
563 2021).
564 *L. rhamnosus* P118 tryptophan-associated enzymes were identified as previously
565 described (including TNA, TMO, TrpD, ArAT, ALD, IPDC, FldH, and AmiE)
566 (Montgomery et al., 2022). Briefly, enzyme commission numbers, where available, or
567 alternatively enzyme names, were queried in PATRIC, PATRIC Global Family (PGF)
568 cross-genus identifiers were extracted and compiled for query within the *L. rhamnosus*
569 P118 genome. Protein sequences of *L. rhamnosus* P118 identified enzymes were
570 analyzed using InterProScan for additional functional prediction, and sequence
571 homology to the previously experimentally validated enzymes within other bacterial
572 species was determined using Blastp at 30% cross-genus identify and 90% identity

573 within each species.

574 ***S.* Typhimurium murine infection model**

575 Animal assays, specifically eighty 6-week-old female C57BL/6 mice (Slac Animal Inc.,
576 Shanghai, China), were conducted in the Laboratory Animal Center of Zhejiang
577 University under light-controlled (12h light/dark cycle), temperature-controlled (22 ±
578 2°C) and humidity-controlled (55 ± 5°C) conditions. Forty mice were randomly
579 selected for survival evaluation under *S*. Typhimurium infection, and the rest were used
580 for sample collection on day 3 post-infection (Figure 2A). The mice were randomly
581 divided into four groups (n = 10/group): Control group (C), *L. rhamnosus* P118 group
582 (P), *S*. Typhimurium-infected group (S), and *L. rhamnosus* P118 protective group (P+S).
583 Mice in the C and S groups were drinking sterile water every day, respectively. Mice
584 in the P and P+ST groups were orally administered with *L. rhamnosus* P118 (1×10^8
585 CFU/mouse) daily for seven days. After that, mice were orally ingested with *S.*
586 Typhimurium SL1344 (1×10^8 CFU/mouse) or sterile PBS. All mice were allowed free
587 access to water and food, and weighed every day. Mice were euthanized on day 3 post-
588 infection. Spleen and liver were weighted for organ index calculation according to the
589 formula: organ index = organ weight (g) / body weight (g) *1000.

590 To evaluate the protective effect of indole-3-acrylic acid (IAA), eighteen mice were
591 randomly divided into three groups (n = 6/group): Control group (C), *S*. Typhimurium-
592 infected group (S), and indole-3-acrylic acid protective group (IAA+S). Mice in the C
593 and S groups were drinking sterile water every day, respectively. IAA (Sigma, I3807)
594 was dissolved in 1 M NaOH in PBS and adjusted pH to 7.4 with 1 M HCl. Mice in the

595 IAA+ST groups were orally administered with 75mg/kg IAA daily for seven days. After
596 that, mice were orally ingested with *S.* Typhimurium SL1344 or sterile PBS. At 3 day-
597 post-infection, mice were euthanized for sample collection.

598 ***In vivo* macrophage depletion**

599 To evaluate the involved roles of macrophages, macrophage depletion assay was
600 conducted through intraperitoneal injection with 250 μL/mouse clodronate liposomes
601 (CLP, From Vrije Universiteit Amsterdam) twice (2 days prior and 1 day after
602 *Salmonella* infection, separately) according to the manufacturer's instructions. Thirty-
603 three mice were randomly divided into six groups (n = 3~6/group): Control group (C),
604 *S.* Typhimurium-infected group (S), Control group with macrophage depletion
605 (CLP+C), *S.* Typhimurium-infected group with macrophage depletion (CLP+S), IAA
606 protective group with macrophage depletion (CLP+IAA+S), and P118 protective group
607 with macrophage depletion (CLP+P+S). At 3 day-post-infection, mice were euthanized
608 for sample collection.

609 **Macrophage cell culture**

610 Murine macrophage cell line RAW 264.7 was cultured in DMEM/F12 medium (Gibco,
611 Carlsbad, CA) supplemented with 10% FBS (Gibco, CA) and 1% (v/v) antibiotic
612 solution (100 μg/mL streptomycin + 100 U/mL penicillin, Sigma-Aldrich, St. Louis,
613 MO) at 37°C in a 5% humidified CO_2 incubator. If not mentioned, the antibiotic
614 solution (100 μg/mL streptomycin and 100 U/mL penicillin) was not added into
615 DMEM/F12 medium in the further experiment.

616 For *S.* Typhimurium killing assay, RAW 264.7 cells seeded into 12-well plates (2 ×

617 10^{6} cells/well) were treated with 100 μM IAA for 6h, followed by infecting with *S.*
618 Typhimurium (MOI = 10) for 1h. After washing 3 times with sterile PBS, the infected
619 RAW 264.7 cells were incubated for 0h, 6h and 12h in DMEM/F12 medium containing
620 gentamicin (50 μg/mL). At each time point, the infected RAW 264.7 cells were washed
621 with sterile PBS for 4 times and lysed with 0.01% Triton X-100 diluted in PBS. The
622 serial 10-fold dilutions of cell lysates were immediately plated on LB agar plates to
623 determine bacterial viability.
624 For the immune response assay, RAW 264.7 cells seeded into 12-well plates (2×10^{6}
625 cells/well) were pretreated with CH-223191 (AHR inhibitor, 10 μM) for 6h,
626 subsequently treating cells with 100 μM IAA for another 6h. After 6h, RAW 264.7 cells
627 were infected with *S.* Typhimurium (MOI = 10) for 2h. After washing 3 times with
628 sterile PBS, the infected RAW 264.7 cells were collected using RNAiso Plus (TaKaRa,
629 Dalian, China) for total RNA extracting and quantitative real-time PCR (qPCR). The
630 primer sets are listed in Table S6.

631 ***S.* Typhimurium burden**

632 *S.* Typhimurium loads in tissues (duodenum, cecum, colon, liver and spleen) and
633 shedding in feces were determined as previously described (Xu et al., 2018). Briefly,
634 tissues and fecal samples were collected under sterile conditions and homogenized in
635 sterile PBS containing 0.1% Triton X-100. Serial 10-fold dilutions of tissue
636 homogenates were spread onto SS agar plates in triplicate and then incubated at 37°C
637 overnight to quantify the bacterial colony-forming unit (CFU).

638 **Histopathology, immunofluorescent analysis, transmission electron microscope**

639 **(TEM) observation and clinical symptom score**

640 Tissues (ileum, liver and spleen) fixed in 4% paraformaldehyde were embedded in
641 paraffin, sliced, dehydrated and then sectioned for hematoxylin and eosin (H&E)
642 staining. The tissue slices were imaged and analyzed by using Olympus Microscope
643 (Tokyo, Japan). For the immunofluorescent assay, the paraffin-embedded ileum
644 samples were incubated with primary antibodies against Ki67 (GB121141, Servicebio,
645 China), lysozyme (GB11345, Servicebio, China), Muc2 (GB11344, Servicebio, China),
646 F4/80 (GB113373, Servicebio, China), iNOS (GB11119, Servicebio, China), IL-1β
647 (GB11113, Servicebio, China), IL-6 (GB11117, Servicebio, China), TNF-α (GB11188,
648 Servicebio, China) for overnight at 4°C and then further incubated with secondary
649 antibodies (Alexa Fluor® 488-conjugated goat anti-rabbit/mouse IgG) or HRP-
650 conjugated goat anti-rabbit secondary antibody (GB23303, Servicebio, China) for 60
651 min at room temperature. Finally, ileum slices were digitalized by Pannoramic MIDI
652 (3DHISTECH, Hungary).

653 TEM observations of ileum tissues were prepared according to our previous study
654 (Peng et al., 2022). Briefly, after being fixed with 2.5% buffered glutaraldehyde, ileum
655 segments were washed three times by cold 100-mM phosphate buffers, and then post-
656 fixed in 0.1% osmium tetroxide for 2 h, rapidly dehydrated in ascending grades of
657 ethanol (30, 50, 70, 95, and 100%), and moved into a 1:1 mixture of propylene oxide
658 and epoxy araldite. Finally, the ileum samples were observed and captured by the
659 transmission electron microscope (JEOL, Tokyo, Japan).

660 The clinical symptom scores were evaluated and graded by two blinded assessors

661 according to previous reported with modified (Burkholder et al., 2012), and the scoring
662 criteria are list in Table S7.

663 **ELISA assay and qPCR**

664 The serum contents of interleukin (IL)-1β and IL-18 were determined by ELISA kits
665 (Solarbio, Beijing, China) according to the manufacturer's instructions.
666 Total RNA extracted from intestinal tissues and RAW 264.7 cells by RNAiso Plus kit
667 (TAKARA, Dalian, China) was reverse-transcripted using PrimeScript II 1st Strand
668 cDNA Synthesis Kit (TAKARA, Dalian, China) according to the manufacturer's
669 instructions. The qPCR was then performed on the StepOne real-time PCR system
670 (Applied Biosystems) using SYBR PremixEx TaqII (TAKARA). The primer sets are
671 listed in Table S6. Fold changes were calculated after normalizing to the housekeeping
672 gene β-actin using the $2^{-\Delta\Delta Ct}$ method (Livak and Schmittgen, 2001).

673 **Microbiota analysis**

674 The TIANamp Stool DNA Kit (Tiangen, Beijing, China) was employed to extract fecal
675 bacterial genomic DNA, and fecal bacterial communities were investigated using 16S
676 rDNA sequencing by targeting the V3-V4 hypervariable region. The 16S rDNA
677 sequencing was then performed on an Illumina NovaSeq platform (Illumina Inc., San
678 Diego, CA, USA). The quality filter of the paired-end raw sequences and a cluster of
679 the filtered sequences into the operational taxonomic unit (OTU) at 97% similarity was
680 performed by QIIME software (version 1.9.1). Microbial OTU representative
681 sequences were assigned to a taxonomic lineage by the RDP classifier based on the
682 SILVA database (v 132 release).

683 To investigate the dissimilarities in bacterial communities and fecal metabolomes,
684 principal coordinates analysis (PCoA), analysis of similarities (ANOSIM),
685 permutational multivariate analysis of variance (PERMANOVA) and multi-response
686 permutation procedure (MRPP) were calculated using "vegan" package and visualized
687 using "ggplot2" package. Difference analysis of bacterial communities based on OUT
688 levels among groups was calculated using "DESeq2" package and was envisioned by
689 "UpSetR" and "ggplot2" packages. The significant differences in bacterial taxonomies
690 were analyzed and visualized by statistical analysis of taxonomic and functional
691 profiles (STAMP) software with a two-sided Welch's t-test (Parks et al., 2014).
692 The sloan neutral model was employed to estimate the importance of neutral processes
693 in the assembly of bacterial communities using "MicEco" package (Sloan et al., 2006).
694 A null-model-based statistical framework was conducted to evaluate the relative
695 importance of determinism and stochasticity in bacterial community assembly (Stegen
696 et al., 2013; Xu et al., 2022). Two assembly processes were defined as deterministic
697 processes ($|\beta NTI|>2$) and stochastic processes ($|\beta NTI|\leq 2$) based on the absolute values
698 of beta Nearest Taxon Index (βNTI) (Xu et al., 2020). Additionally, five ecological
699 assembly processes were then interpreted as homogeneous selection ($\beta NTI<-2$),
700 homogenizing dispersal ($|\beta NTI|\leq 2$ and $RC_{bray}<-0.95$), undominated ($|\beta NTI|\leq 2$ and
701 $|RC_{bray}|<0.95$), dispersal limitation ($|\beta NTI|\leq 2$ and $RC_{bray}>0.95$) and variable
702 (heterogeneous) selection ($\beta NTI>2$) based on the threshold of the absolute values of
703 βNTI and Bray-Curtis-based Raup-Crick (RC_{bray}) (Jiao et al., 2020; Xu et al., 2022).
704 **Metabolomics analysis**

705 Untargeted metabolomics was investigated to analyze the fecal metabolomes of mice.
706 The method for extracting metabolites from feces was conducted according to our
707 previous study described (Wang et al., 2021b). After extracting metabolites from feces,
708 UHPLC-MS/MS analyses of samples were performed by Vanquish UHPLC systems
709 (Thermo Fisher, Germany) coupled with Orbitrap Q Exactive^{TM} HF-X mass
710 spectrometers (Thermo Fisher, Germany) in Novogene Co., Ltd. (Beijing, China).
711 Compound Discoverer 3.1 (CD3.1, Thermo Fisher) was employed to conduct peak
712 alignment, and quantify metabolites generated by UHPLC-MS/MS. After normalizing
713 to total spectral intensity and predicting molecular formula, the peaks were queried
714 against mzCloud, mzVault and MassList databases to extract the quantitative results.
715 Annotation of fecal metabolite signatures was queried against the KEGG database,
716 HMDB database and LIPIDMaps database. Significant differences in fecal metabolites
717 were analyzed using univariate analysis (t-test) and partial least-squares discriminant
718 analysis (PLS-DA), in which fecal metabolites with variable importance in the
719 projection (VIP) > 1 and $P < 0.05$ were considered differential metabolites. Pearson
720 correlation analysis between *S*. Typhimurium burden (in tissues and feces) and fecal
721 metabolites was analyzed and visualized using "linkET" package (Huang, 2021).
722 MetOrigin platform was employed to analyze the sources of microbial metabolites and
723 their metabolic functions in fecal metabolomes (Yu et al., 2022).

724 **Statistical Analysis**

725 The significance of the results was analyzed by one-way analysis of variance (ANOVA)
726 with Tukey's multiple comparisons test using SPSS v24 (SPSS Inc., Chicago, IL, USA)

727 and statistical graphs were visualized by GraphPad Prism v8.0 (GraphPad Software,
728 CA) and package "ggplot2" of R software (v4.3.1). * $P < 0.05$, ** $P < 0.01$, *** $P <$
729 0.001.
730

731 **Acknowledgements**

732 This work was supported by the National Program on Key Research Project of China
733 (2022YFC2604201) as well as the European Union's Horizon 2020 Research and
734 Innovation Programme under Grant Agreement No. 861917-SAFFI, Zhejiang
735 Provincial Key R&D Program of China (2023C03045, 2022C02024), Key Research
736 and Development Program of Hangzhou (202203A08), Zhejiang Provincial Natural
737 Science Foundation of China (LQ23C180005).

738 **Conflict of interest statement**

739 No potential conflict of interest was reported by the author(s).

740 **Data availability statement**

741 16S rRNA sequencing data is deposited at the Genome Sequence Archive (GSA) of the
742 BIG Data Center (https://bigd.big.ac.cn/gsa/) under accession no. PRJCA021751. *L.*
743 *rhamnosus* P118 isolate draft genome assembly is publicly available in the NCBI under
744 accession no. PRJNA848987.

745 **Ethics statement**

746 Animal procedures followed the guidelines and were approved by the Institutional
747 Animal Care and Use Committee of Zhejiang University (Permission number:
748 ZJU20220295).

749 **Author contributions**

750 Baikui Wang and Xianqi Peng: Investigation, Validation, Methodology, Data Analysis,
751 Visualization, Formal analysis, Writing - original draft & review & editing; Xiao Zhou,
752 Jiayun Yao, Haiqi Zhang, Weifen Li, Yan Li: Investigation, Writing – review; Min Yue:
753 Conceptualization, Resources, Methodology, Supervision, Writing – review & editing,
754 Funding acquisition, Project administration.

755 **References**

756 Agus A, Planchais J, Sokol H. Gut microbiota regulation of tryptophan metabolism in
757 health and disease. Cell Host Microbe 2018;23:716-24.

758 Bernal-Bayard J, Ramos-Morales F. Molecular mechanisms used by salmonella to
759 evade the immune system. Curr Issues Mol Biol 2018;25:133-68.

760 Britton GJ, Faith JJ. Causative microbes in host-microbiome interactions. Annu Rev
761 Microbiol 2021;75:223-42.

762 Burkholder T, Foltz C, Karlsson E, Linton CG, Smith JM. Health evaluation of
763 experimental laboratory mice. Curr Protoc Mouse Biol 2012;2:145-65.

764 Caballero-Flores G, Pickard JM, Nunez G. Microbiota-mediated colonization
765 resistance: Mechanisms and regulation. Nat Rev Microbiol 2022.

766 Caballero-Flores G, Pickard JM, Nunez G. Microbiota-mediated colonization
767 resistance: Mechanisms and regulation. Nat Rev Microbiol 2023;21:347-60.

768 Cani PD. Microbiota and metabolites in metabolic diseases. Nat Rev Endocrinol
769 2019;15:69-70.

770 Cervantes-Barragan L, Chai JN, Tianero MD, Di Luccia B, Ahern PP, Merriman J,
771 Cortez VS, Caparon MG, Donia MS, Gilfillan S, Cella M, Gordon JI, Hsieh CS,
772 Colonna M. Lactobacillus reuteri induces gut intraepithelial
773 cd4(+)cd8alphaalpha(+) t cells. Science 2017;357:806-10.

774 Dong N, Yang X, Chan EW, Zhang R, Chen S. Klebsiella species: Taxonomy,
775 hypervirulence and multidrug resistance. EBioMedicine 2022;79:103998.

776 Eng SK, Pusparajah P, Ab Mutalib NS, Ser HL, Chan KG, Lee LH. Salmonella: A
777 review on pathogenesis, epidemiology and antibiotic resistance. Frontiers in
778 Life Science 2015;8:284-93.
779 Fishbein SRS, Mahmud B, Dantas G. Antibiotic perturbations to the gut microbiome.
780 Nat Rev Microbiol 2023;21:772-88.
781 Fu A, Mo Q, Wu Y, Wang B, Liu R, Tang L, Zeng Z, Zhang X, Li W. Protective effect
782 of bacillus amyloliquefaciens against salmonella via polarizing macrophages to
783 m1 phenotype directly and to m2 depended on microbiota. Food & function
784 2019;10:7653-66.
785 Galan JE. Salmonella typhimurium and inflammation: A pathogen-centric affair. Nat
786 Rev Microbiol 2021;19:716-25.
787 Gareau MG, Sherman PM, Walker WA. Probiotics and the gut microbiota in intestinal
788 health and disease. Nat Rev Gastroenterol Hepatol 2010;7:503-14.
789 Gillis CC, Hughes ER, Spiga L, Winter MG, Zhu W, Furtado De Carvalho T, Chanin
790 RB, Behrendt CL, Hooper LV, Santos RL, Winter SE. Dysbiosis-associated
791 change in host metabolism generates lactate to support salmonella growth. Cell
792 Host Microbe 2018a;23:54-64 e6.
793 Gillis CC, Hughes ER, Spiga L, Winter MG, Zhu W, Furtado De Carvalho T, Chanin
794 RB, Behrendt CL, Hooper LV, Santos RL, Winter SE. Dysbiosis-associated
795 change in host metabolism generates lactate to support salmonella growth. Cell
796 Host Microbe 2018b;23:570.
797 Girard LR, Fiedler TJ, Harris TW, Carvalho F, Antoshechkin I, Han M, Sternberg PW,
798 Stein LD, Chalfie M. Wormbook: The online review of caenorhabditis elegans
799 biology. Nucleic Acids Res 2007;35:D472-5.
800 He D, Zeng W, Wang Y, Xing Y, Xiong K, Su N, Zhang C, Lu Y, Xing X. Isolation and
801 characterization of novel peptides from fermented products of lactobacillus for
802 ulcerative colitis prevention and treatment. Food Science and Human Wellness
803 2022;11:1464-74.
804 Hiyoshi H, English BC, Diaz-Ochoa VE, Wangdi T, Zhang LF, Sakaguchi M, Haneda
805 T, Tsolis RM, Baumler AJ. Virulence factors perforate the pathogen-containing

806 vacuole to signal efferocytosis. Cell Host Microbe 2022;30:163-70 e6.
807 Huang H. Linket: Everything is linkable. R package version 0.0.3 2021.
808 Hudzicki J. Kirby-bauer disk diffusion susceptibility test protocol. American society
809 for microbiology 2009;15:55-63.
810 Iram D, Kindarle UA, Sansi MS, Meena S, Puniya AK, Vij S. Peptidomics-based
811 identification of an antimicrobial peptide derived from goat milk fermented by
812 lactobacillus rhamnosus (c25). J Food Biochem 2022;46:e14450.
813 Jacobson A, Lam L, Rajendram M, Tamburini F, Honeycutt J, Pham T, Van Treuren W,
814 Pruss K, Stabler SR, Lugo K, Bouley DM, Vilches-Moure JG, Smith M,
815 Sonnenburg JL, Bhatt AS, Huang KC, Monack D. A gut commensal-produced
816 metabolite mediates colonization resistance to salmonella infection. Cell Host
817 Microbe 2018;24:296-307 e7.
818 Jiao S, Yang YF, Xu YQ, Zhang J, Lu YH. Balance between community assembly
819 processes mediates species coexistence in agricultural soil microbiomes across
820 eastern china. Isme Journal 2020;14:202-16.
821 Jiao S, Zhang B, Zhang G, Chen W, Wei G. Stochastic community assembly decreases
822 soil fungal richness in arid ecosystems. Mol Ecol 2021;30:4338-48.
823 Kankainen M, Paulin L, Tynkkynen S, Von Ossowski I, Reunanen J, Partanen P,
824 Satokari R, Vesterlund S, Hendrickx AP, Lebeer S, De Keersmaecker SC,
825 Vanderleyden J, Hamalainen T, Laukkanen S, Salovuori N, Ritari J, Alatalo E,
826 Korpela R, Mattila-Sandholm T, Lassig A, Hatakka K, Kinnunen KT,
827 Karjalainen H, Saxelin M, Laakso K, Surakka A, Palva A, Salusjarvi T, Auvinen
828 P, De Vos WM. Comparative genomic analysis of lactobacillus rhamnosus gg
829 reveals pili containing a human- mucus binding protein. Proc Natl Acad Sci U
830 S A 2009;106:17193-8.
831 Kim HB, Isaacson RE. Salmonella in swine: Microbiota interactions. Annual Review
832 of Animal Biosciences, Vol 5 2017;5:43-63.
833 Koh A, Backhed F. From association to causality: The role of the gut microbiota and its
834 functional products on host metabolism. Mol Cell 2020;78:584-96.
835 Kumar A, Baruah A, Tomioka M, Iino Y, Kalita MC, Khan M. Caenorhabditis elegans:

836 A model to understand host-microbe interactions. Cell Mol Life Sci
837 2020;77:1229-49.
838 Laupland KB, Paterson DL, Edwards F, Stewart AG, Harris PNA. Morganella morganii,
839 an emerging cause of bloodstream infections. Microbiol Spectr
840 2022;10:e0056922.
841 Lavelle A, Sokol H. Gut microbiota-derived metabolites as key actors in inflammatory
842 bowel disease. Nature Reviews Gastroenterology & Hepatology 2020;17:223-
843 37.
844 Letunic I, Bork P. Interactive tree of life (itol) v5: An online tool for phylogenetic tree
845 display and annotation. Nucleic acids research 2021;49:W293-W6.
846 Levy M, Kolodziejczyk AA, Thaiss CA, Elinav E. Dysbiosis and the immune system.
847 Nat Rev Immunol 2017;17:219-32.
848 Liu J, Liu H, Liu H, Teng Y, Qin N, Ren X, Xia X. Live and pasteurized akkermansia
849 muciniphila decrease susceptibility to salmonella typhimurium infection in
850 mice. J Adv Res 2023;52:89-102.
851 Livak KJ, Schmittgen TD. Analysis of relative gene expression data using real-time
852 quantitative pcr and the 2(t)(-delta delta c) method. Methods 2001;25:402-8.
853 Montgomery TL, Eckstrom K, Lile KH, Caldwell S, Heney ER, Lahue KG,
854 D'alessandro A, Wargo MJ, Krementsov DN. Lactobacillus reuteri tryptophan
855 metabolism promotes host susceptibility to cns autoimmunity. Microbiome
856 2022;10:198.
857 Na YR, Stakenborg M, Seok SH, Matteoli G. Macrophages in intestinal inflammation
858 and resolution: A potential therapeutic target in ibd. Nat Rev Gastroenterol
859 Hepatol 2019;16:531-43.
860 Neurath MF. Strategies for targeting cytokines in inflammatory bowel disease. Nat Rev
861 Immunol 2024.
862 Olesen SW, Barnett ML, Macfadden DR, Brownstein JS, Hernandez-Diaz S, Lipsitch
863 M, Grad YH. The distribution of antibiotic use and its association with antibiotic
864 resistance. Elife 2018;7.
865 Olive AJ, Sassetti CM. Metabolic crosstalk between host and pathogen: Sensing,

adapting and competing. Nature Reviews Microbiology 2016;14:221-34.

Parks DH, Tyson GW, Hugenholtz P, Beiko RG. Stamp: Statistical analysis of taxonomic and functional profiles. Bioinformatics 2014;30:3123-4.

Peng X, Ed-Dra A, Song Y, Elbediwi M, Nambiar RB, Zhou X, Yue M. Lacticaseibacillus rhamnosus alleviates intestinal inflammation and promotes microbiota-mediated protection against salmonella fatal infections. Front Immunol 2022;13:973224.

Poupet C, Chassard C, Nivoliez A, Bornes S. Caenorhabditis elegans, a host to investigate the probiotic properties of beneficial microorganisms. Front Nutr 2020;7:135.

Rangan KJ, Pedicord VA, Wang YC, Kim B, Lu Y, Shaham S, Mucida D, Hang HC. A secreted bacterial peptidoglycan hydrolase enhances tolerance to enteric pathogens. Science 2016;353:1434-7.

Read E, Curtis MA, Neves JF. The role of oral bacteria in inflammatory bowel disease. Nat Rev Gastroenterol Hepatol 2021;18:731-42.

Rodriguez-R LM, Konstantinidis KT, The enveomics collection: A toolbox for specialized analyses of microbial genomes and metagenomes. PeerJ Preprints; 2016.p.

Rodriguez RL, Gunturu S, Harvey WT, Rossello-Mora R, Tiedje JM, Cole JR, Konstantinidis KT. The microbial genomes atlas (miga) webserver: Taxonomic and gene diversity analysis of archaea and bacteria at the whole genome level. Nucleic Acids Res 2018;46:W282-W8.

Rogers AP, Mileto SJ, Lyras D. Impact of enteric bacterial infections at and beyond the epithelial barrier. Nature Reviews Microbiology 2022.

Sakandar HA, Zhang HP. Trends in probiotic(s)-fermented milks and their in vivo functionality: A review. Trends in Food Science & Technology 2021;110:55-65.

Sanders ME, Merenstein DJ, Reid G, Gibson GR, Rastall RA. Probiotics and prebiotics in intestinal health and disease: From biology to the clinic. Nat Rev Gastroenterol Hepatol 2019;16:605-16.

Schwarze K, Buchanan J, Fermont JM, Dreau H, Tilley MW, Taylor JM, Antoniou P,

896 Knight SJL, Camps C, Pentony MM, Kvikstad EM, Harris S, Popitsch N,
897 Pagnamenta AT, Schuh A, Taylor JC, Wordsworth S. The complete costs of
898 genome sequencing: A microcosting study in cancer and rare diseases from a
899 single center in the united kingdom. Genet Med 2020;22:85-94.
900 Shi J, Yang L, Liao Y, Li J, Jiao S, Shangguan Z, Deng L. Soil labile organic carbon
901 fractions mediate microbial community assembly processes during long-term
902 vegetation succession in a semiarid region. iMeta 2023:e142.
903 Sloan WT, Lunn M, Woodcock S, Head IM, Nee S, Curtis TP. Quantifying the roles of
904 immigration and chance in shaping prokaryote community structure. Environ
905 Microbiol 2006;8:732-40.
906 Stanaway JD, Parisi A, Sarkar K, Blacker BF, Reiner RC, Hay SI, Nixon MR, Dolecek
907 C, James SL, Mokdad AH, Abebe G, Ahmadian E, Alahdab F, Alemnew BT,
908 Alipour V, Bakeshei FA, Animut MD, Ansari F, Arabloo J, Asfaw ET,
909 Bagherzadeh M, Bassat Q, Belayneh YM, Carvalho F, Daryani A, Demeke FM,
910 Demis AB, Dubey M, Duken EE, Dunachie SJ, Eftekhari A, Fernandes E, Fard
911 RF, Gedefaw GA, Geta B, Gibney KB, Hasanzadeh A, Hoang CL, Kasaeian A,
912 Khater A, Kidanemariam ZT, Lakew AM, Malekzadeh R, Melese A, Mengistu
913 DT, Mestrovic T, Miazgowski B, Mohammad KA, Mohammadian M,
914 Mohammadian-Hafshejani A, Nguyen T, Nguyen H, Nguyen H, Nirayo YL,
915 Olagunju AT, Olagunju TO, Pourjafar H, Qorbani M, Rabiee M, Rabiee N,
916 Rafay A, Rezapour A, Samy AM, Sepanlou SG, Shaikh MA, Sharif M,
917 Shigematsu M, Tessema B, Tran BX, Ullah I, Yimer EM, Zaidi Z, Murray CJL,
918 Crump JA, Salm GN-T. The global burden of non-typhoidal salmonella invasive
919 disease: A systematic analysis for the global burden of disease study 2017.
920 Lancet Infectious Diseases 2019;19:1312-24.
921 Stegen JC, Lin X, Konopka AE, Fredrickson JK. Stochastic and deterministic assembly
922 processes in subsurface microbial communities. ISME J 2012;6:1653-64.
923 Stegen JC, Lin XJ, Fredrickson JK, Chen XY, Kennedy DW, Murray CJ, Rockhold ML,
924 Konopka A. Quantifying community assembly processes and identifying
925 features that impose them. Isme Journal 2013;7:2069-79.

926 Sun Y, Li HC, Zheng L, Li JZ, Hong Y, Liang PF, Kwok LY, Zuo YC, Zhang WY, Zhang
927 HP. Iprobiotics: A machine learning platform for rapid identification of
928 probiotic properties from whole-genome primary sequences. Briefings in
929 Bioinformatics 2022;23.
930 Thiagarajah JR, Donowitz M, Verkman AS. Secretory diarrhoea: Mechanisms and
931 emerging therapies. Nat Rev Gastroenterol Hepatol 2015;12:446-57.
932 Unicef, Diarrhoea remains a leading killer of young children, despite the availability of
933 a simple treatment solution. U Data (Ed.). https://data.unicef.org/topic/child-
934 health/diarrhoeal-disease/; 2022.p.
935 Vellend M. Conceptual synthesis in community ecology. Q Rev Biol 2010;85:183-206.
936 Wan MLY, Forsythe SJ, El-Nezami H. Probiotics interaction with foodborne pathogens:
937 A potential alternative to antibiotics and future challenges. Critical reviews in
938 food science and nutrition 2019;59:3320-33.
939 Wang B, Hussain A, Zhou Y, Zeng Z, Wang Q, Zou P, Gong L, Zhao P, Li W.
940 Saccharomyces boulardii attenuates inflammatory response induced by
941 clostridium perfringens via tlr4/tlr15-myd8 pathway in hd11 avian macrophages.
942 Poult Sci 2020;99:5356-65.
943 Wang B, Ye X, Zhou Y, Zhao P, Mao Y. Glycyrrhizin attenuates salmonella
944 typhimurium-induced tissue injury, inflammatory response, and intestinal
945 dysbiosis in c57bl/6 mice. Front Vet Sci 2021a;8:648698.
946 Wang B, Zhou Y, Mao Y, Gong L, Li X, Xu S, Wang F, Guo Q, Zhang H, Li W. Dietary
947 supplementation with lactobacillus plantarum ameliorates compromise of
948 growth performance by modulating short-chain fatty acids and intestinal
949 dysbiosis in broilers under clostridium perfringens challenge. Front Nutr
950 2021b;8:706148.
951 Wang B, Zhou Y, Wang Q, Xu S, Wang F, Yue M, Zeng Z, Li W. Lactiplantibacillus
952 plantarum lac16 attenuates enterohemorrhagic escherichia coli o157:H7
953 infection by inhibiting virulence traits and improving intestinal epithelial barrier
954 function. Cells 2023;12.
955 Wang L, Liu Q, Chen Y, Zheng X, Wang C, Qi Y, Dong Y, Xiao Y, Chen C, Chen T,

956 Huang Q, Zhai Z, Long C, Yang H, Li J, Wang L, Zhang G, Liao P, Liu YX,
957 Huang P, Huang J, Wang Q, Chu H, Yin J, Yin Y. Antioxidant potential of
958 pediococcus pentosaceus strains from the sow milk bacterial collection in
959 weaned piglets. Microbiome 2022;10:83.
960 Who, Diarrhoeal disease. 2017.p.
961 Wlodarska M, Luo C, Kolde R, D'hennezel E, Annand JW, Heim CE, Krastel P, Schmitt
962 EK, Omar AS, Creasey EA, Garner AL, Mohammadi S, O'connell DJ,
963 Abubucker S, Arthur TD, Franzosa EA, Huttenhower C, Murphy LO, Haiser HJ,
964 Vlamakis H, Porter JA, Xavier RJ. Indoleacrylic acid produced by commensal
965 peptostreptococcus species suppresses inflammation. Cell Host Microbe
966 2017;22:25-37 e6.
967 Wu Y, Zhang X, Liu X, Li Y, Han D, Pi Y, Whitmore MA, Lu X, Zhang G, Zheng J,
968 Wang J. Strain specificity of lactobacilli with promoted colonization by
969 galactooligosaccharides administration in protecting intestinal barriers during
970 salmonella infection. J Adv Res 2024;56:1-14.
971 Xiao Y, Zhai Q, Zhang H, Chen W, Hill C. Gut colonization mechanisms of
972 lactobacillus and bifidobacterium: An argument for personalized designs. Annu
973 Rev Food Sci Technol 2021;12:213-33.
974 Xu Q, Ling N, Chen H, Duan Y, Wang S, Shen Q, Vandenkoornhuyse P. Long-term
975 chemical-only fertilization induces a diversity decline and deep selection on the
976 soil bacteria. mSystems 2020;5.
977 Xu Q, Vandenkoornhuyse P, Li L, Guo J, Zhu C, Guo S, Ling N, Shen Q. Microbial
978 generalists and specialists differently contribute to the community diversity in
979 farmland soils. J Adv Res 2022;40:17-27.
980 Xu XG, Gong L, Wang BK, Wu YP, Wang Y, Mei XQ, Xu H, Tang L, Liu RR, Zeng
981 ZH, Mao YL, Li WF. Glycyrrhizin attenuates salmonella enterica serovar
982 typhimurium infection: New insights into its protective mechanism. Frontiers
983 in Immunology 2018;9:2321.
984 Xun W, Li W, Xiong W, Ren Y, Liu Y, Miao Y, Xu Z, Zhang N, Shen Q, Zhang R.
985 Diversity-triggered deterministic bacterial assembly constrains community

986 functions. Nat Commun 2019;10:3833.
987 Yu G, Xu C, Zhang D, Ju F, Ni Y. Metorigin: Discriminating the origins of microbial
988 metabolites for integrative analysis of the gut microbiome and metabolome.
989 IMeta 2022;1:e10.
990 Zhang Y, Wang J, He J, Liu X, Sun J, Song X, Wu Y. Characteristics and application in
991 cheese making of newly isolated milk-clotting enzyme from bacillus
992 megaterium ly114. Food Res Int 2023;172:113202.
993 Zhou J, Ning D. Stochastic community assembly: Does it matter in microbial ecology?
994 Microbiology and Molecular Biology Reviews 2017;81:e00002-17.
995 Zhou X, Kang X, Chen J, Song Y, Jia C, Teng L, Tang Y, Jiang Z, Peng X, Tao X.
996 Genome degradation promotes salmonella pathoadaptation by remodeling
997 fimbriae-mediated proinflammatory response. National Science Review
998 2023:nwad228.
999

Figures

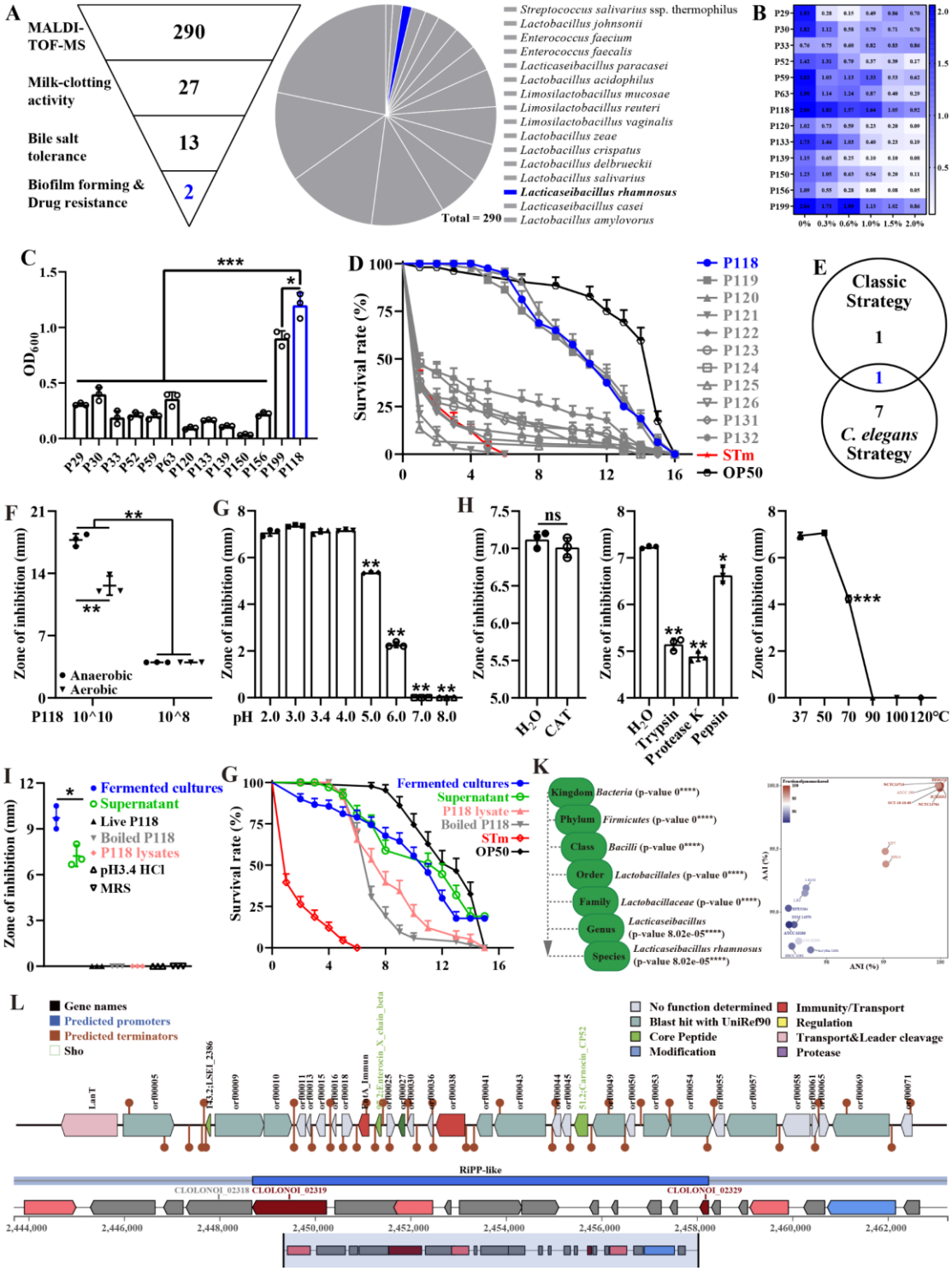

Figure 1. Isolation and antibacterial characterization of *L. rhamnosus* P118. (**A**) Screening flowchart of P118 *in vitro* and candidate probiotic isolates identified by MALDI-TOF MS. (**B**) Bile salt tolerance ability of the isolates. (**C**) Biofilm forming

1005 ability of isolates. (**D**) Screening using *C. elegans* infection model. (**E**) Interacted
1006 screening strategy. (**F**) Antibacterial ability of P118 under aerobic or anaerobic culture
1007 conditions. (**G**) Broad-spectrum pH tolerance of P118 supernatants (pH = 3.4) that
1008 adjusted to pH < 3.4 by 1M HCl or pH > 3.4 by 1M NaOH. (**H**) Antibacterial effects of
1009 P118 supernatant under 20 mg/mL catalase (CAT), 100μg/mL proteinases (trypsin,
1010 proteinase K, pepsin), and different temperatures (37, 50, 70, 90, 100, 120℃) boiled
1011 for 30 min treatments. (**I**) Antibacterial effects of components of P118 (boiled at 120 ℃
1012 for 30 min or was lysed by ultrasonication at 240 W for 2 h). (**G**) Active ingredients of
1013 P118 protect *C. elegans* against *S.* Typhimurium infection. (**K**) Taxonomic
1014 classification of P118 draft genome queried against the NCBI non-redundant
1015 prokaryotic genomes database with p-values representing confidence of phylogenetic
1016 assignment, and the nearest subspecies phylogenetic neighbor of P118 draft genome
1017 was determined by percentage shared genomic content graphed as ANI versus AAI. (**L**)
1018 Prediction of secondary metabolites and bacteriocin protein-encoding gene clusters of
1019 P118 using antiSMASH and BAGEL4 databases. (**F-G**) *S.* Typhimurium SL1344 was
1020 selected as an indicator pathogen. Significant differences * $P < 0.05$, ** $P < 0.01$, ***
1021 $P < 0.001$.

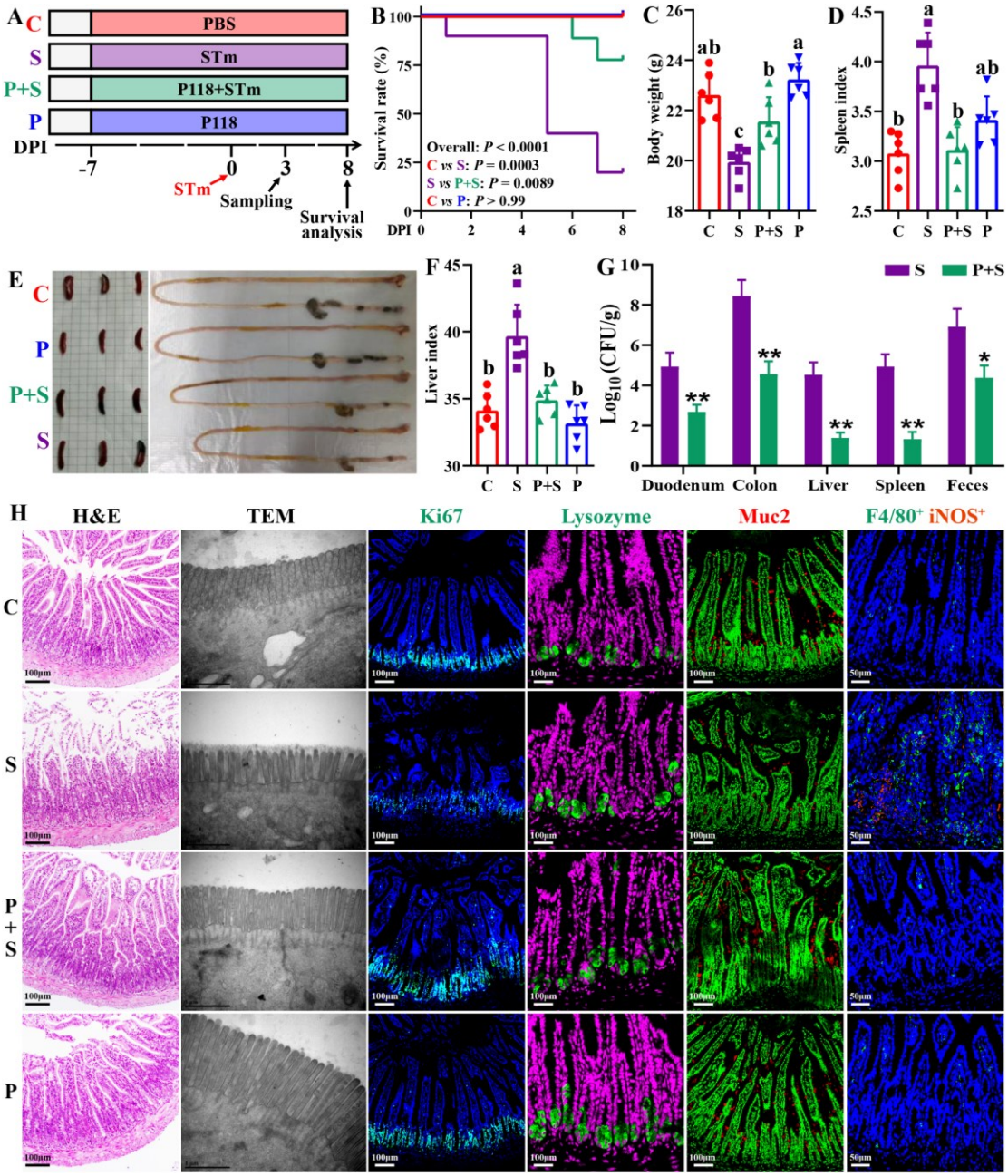

Figure 2. *L. rhamnosus* P118 enhances mice tolerance to *S*. Typhimurium infection. (**A**) Experimental design. (**B**) Survival curve of mice infected with *S*. Typhimurium. (**C**) Body weight. (**D**) Spleen index. (**E**) Representative images of spleen and intestine. (**F**) Liver index. (**G**) *S.* Typhimurium burden in tissues and shedding in feces. (**H**) Representative images of H&E staining, TEM, and immunostaining (DAPI, Ki67, lysozyme, Muc2, F4/80, iNOS) in the ileum. Different lowercase letters indicate a significant difference ($P < 0.05$). Significant differences * $P < 0.05$, ** $P < 0.01$. C:

PBS group; P: P118 administered group; S: *S*. Typhimurium-infected group; P+S: P118 protective group.

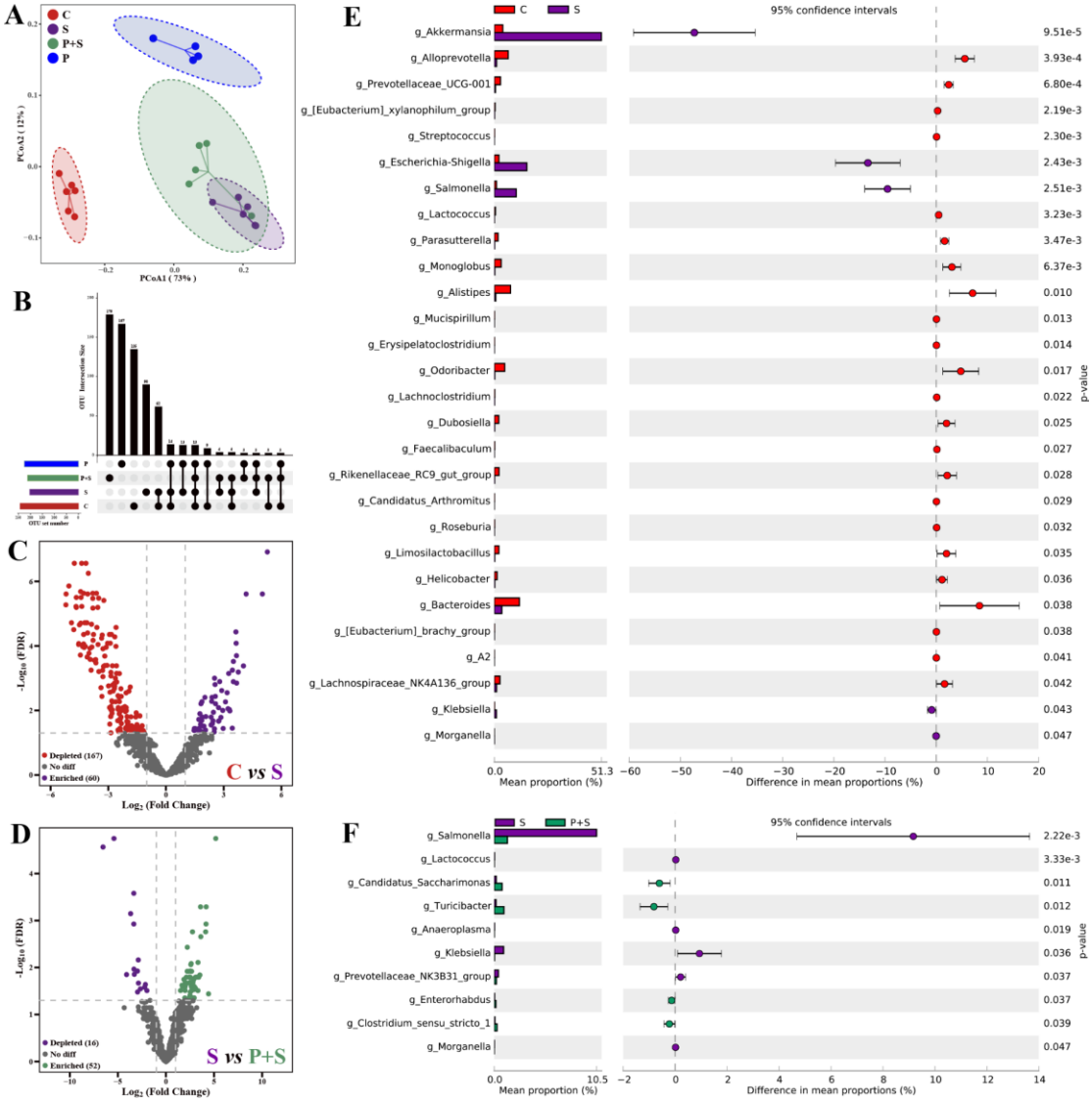

Figure 3. *L. rhamnosus* P118 improves *S*. Typhimurium infection-induced dysbacteriosis. (**A**) Principal coordinates analysis (PCoA) based on Bray-Curtis distance. (**B**) UpSetR plot based on bacterial absolute OTU abundances. (**C & D**) The fold changes of bacterial absolute OTU abundances between two groups. (**E & F**) Comparison of intestinal microbes by STAMP. The prefix "g_" represent the annotated level of the genus. C: PBS group; P: P118 administered group; S: *S*. Typhimurium-infected group; P+S: P118 protective group.

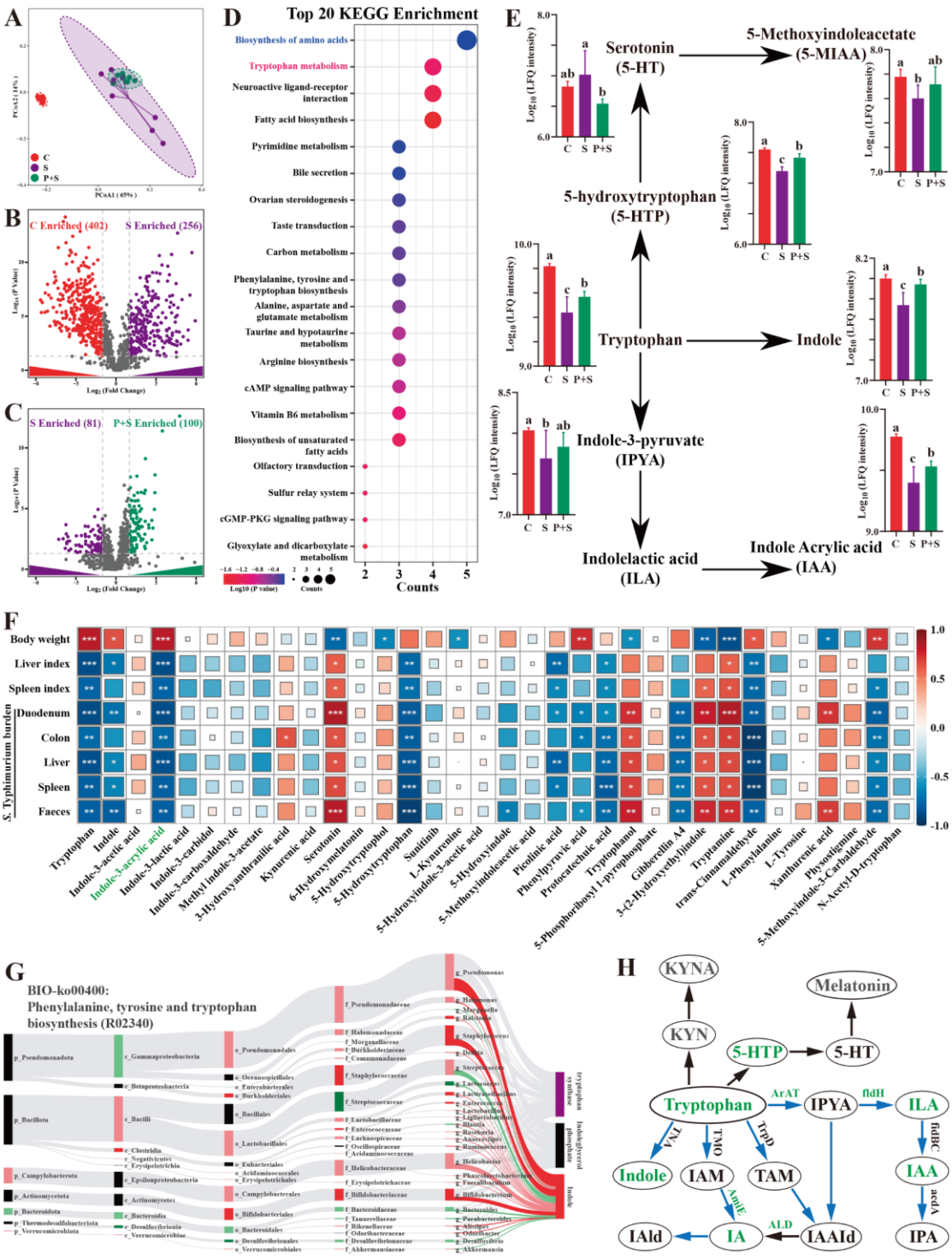

Figure 4. Microbe derived tryptophan metabolites are involved in mice tolerance to *S.* Typhimurium. (**A**) Principal coordinates analysis (PCoA) based on Bray-Curtis distance of fecal metabolites. (**B & C**) UpSetR plot based on fecal metabolites. (**D**) Metabolomics pathway enrichment in "P+S *vs* S". (**E**) Comparison of fecal microbial

tryptophan metabolism enriched pathway among groups. (**F**) Pearson correlation analysis among *S.* Typhimurium burden, organ indices, body weight and fecal metabolites in mice. (**G**) Bio-Sankey network analysis between intestinal microbes and fecal metabolites. (**H**) Pathway schematic of abbreviated mammalian and microbial tryptophan metabolism. Different lowercase letters indicate a significant difference ($P < 0.05$). Significant differences $^{*}P < 0.05$; $^{**}P < 0.01$; $^{***}P < 0.001$. C: PBS group; P: P118 administered group; S: *S.* Typhimurium-infected group; P+S: P118 protective group.

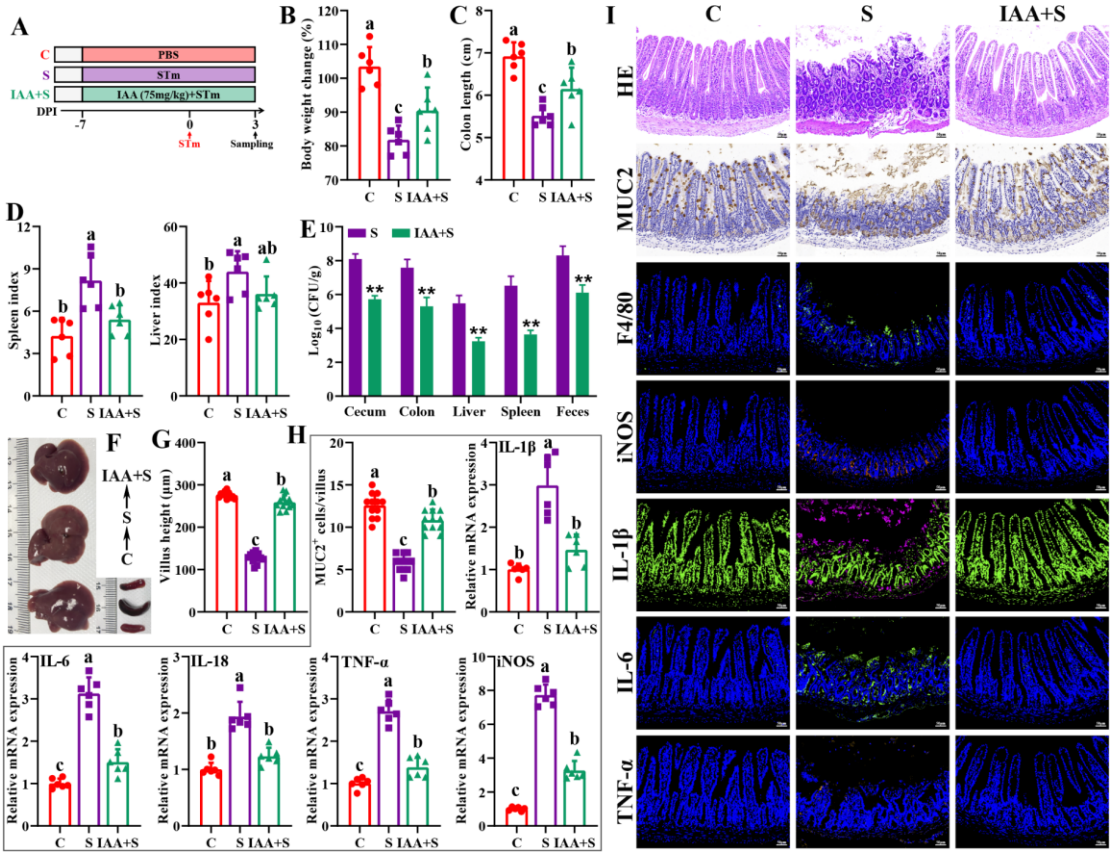

Figure 5. Indole-3-acrylic acid enhances mice tolerance to *S.* Typhimurium infection. (**A**) Experimental design. (**B**) Body weight change. (**C**) Colon length. (**D**) Spleen and liver indexes. (**E**) *S.* Typhimurium burden in tissues and shedding in feces. (**F**) Representative images of spleen and liver. (**G**) Villus height of ileum. (**H**) Muc2-

positive cells and mRNA expression levels in ileum. (**I**) Representative images of H&E staining and immunostaining in the ileum. Different lowercase letters indicate a significant difference ($P < 0.05$). C: PBS group; S: *S.* Typhimurium-infected group; IAA+S: indole-3-acrylic acid protective group.

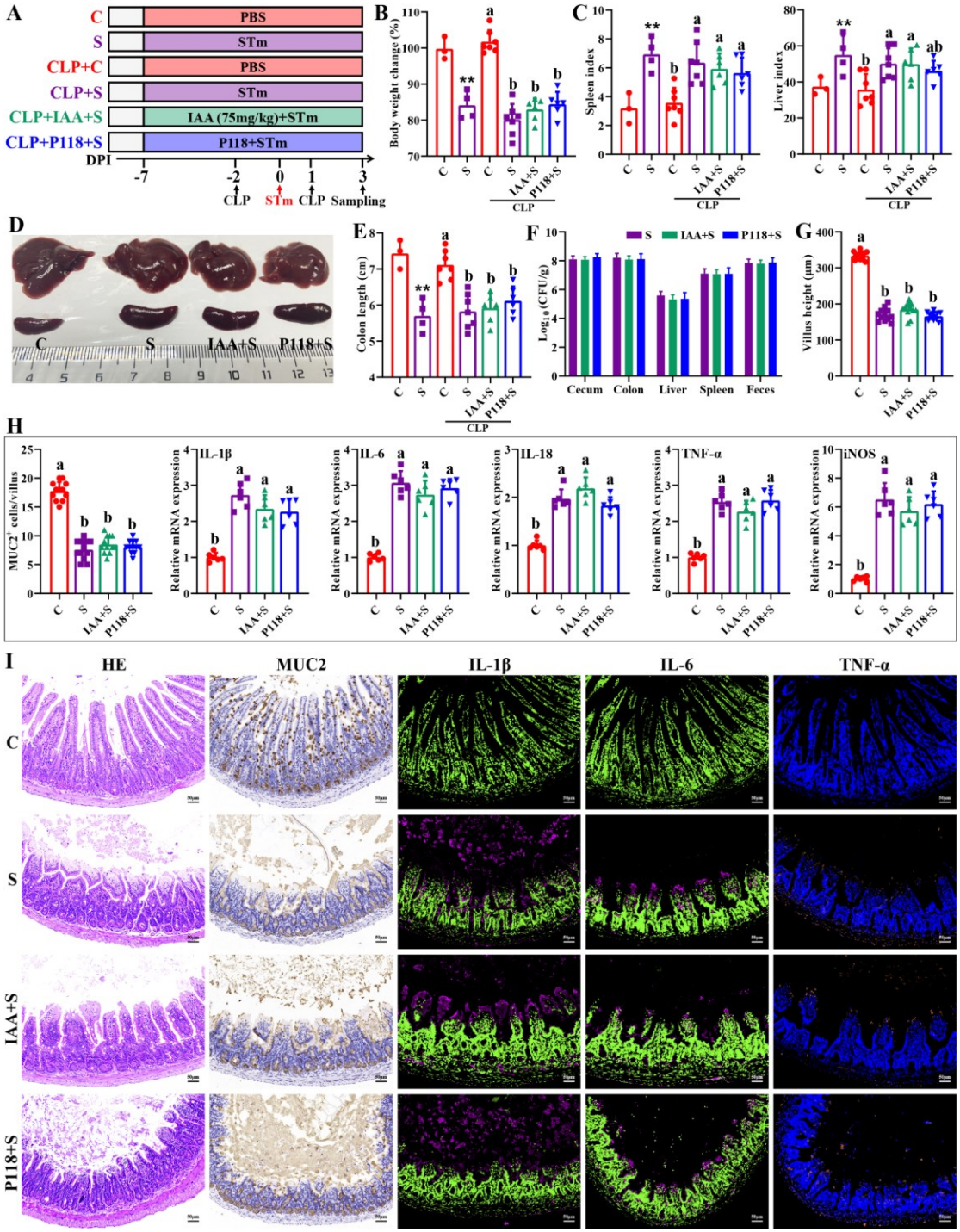

Figure 6. Macrophage depletion abrogates the protective effect of *L. rhamnosus* P118

and indole-3-acrylic acid against *S*. Typhimurium infection. (**A**) Experimental design. (**B**) Body weight change. (**C**) Spleen and liver indexes. (**D**) Representative images of spleen and liver. (**E**) Colon length. (**F**) *S.* Typhimurium burden in tissues and shedding in feces. (**G**) Villus height of ileum. (**H**) Muc2-positive cells and mRNA expression levels in ileum. (**I**) Representative images of H&E staining and immunostaining in the ileum. Different lowercase letters indicate a significant difference ($P < 0.05$). (**B-E**) Significant differences ** $P < 0.01$ indicates "S *vs* C".CLP: macrophage depletion reagent clodronate liposomes. C: PBS group; S: S. Typhimurium-infected group; IAA+S: indole-3-acrylic acid protective group; P+S: P118 protective group.

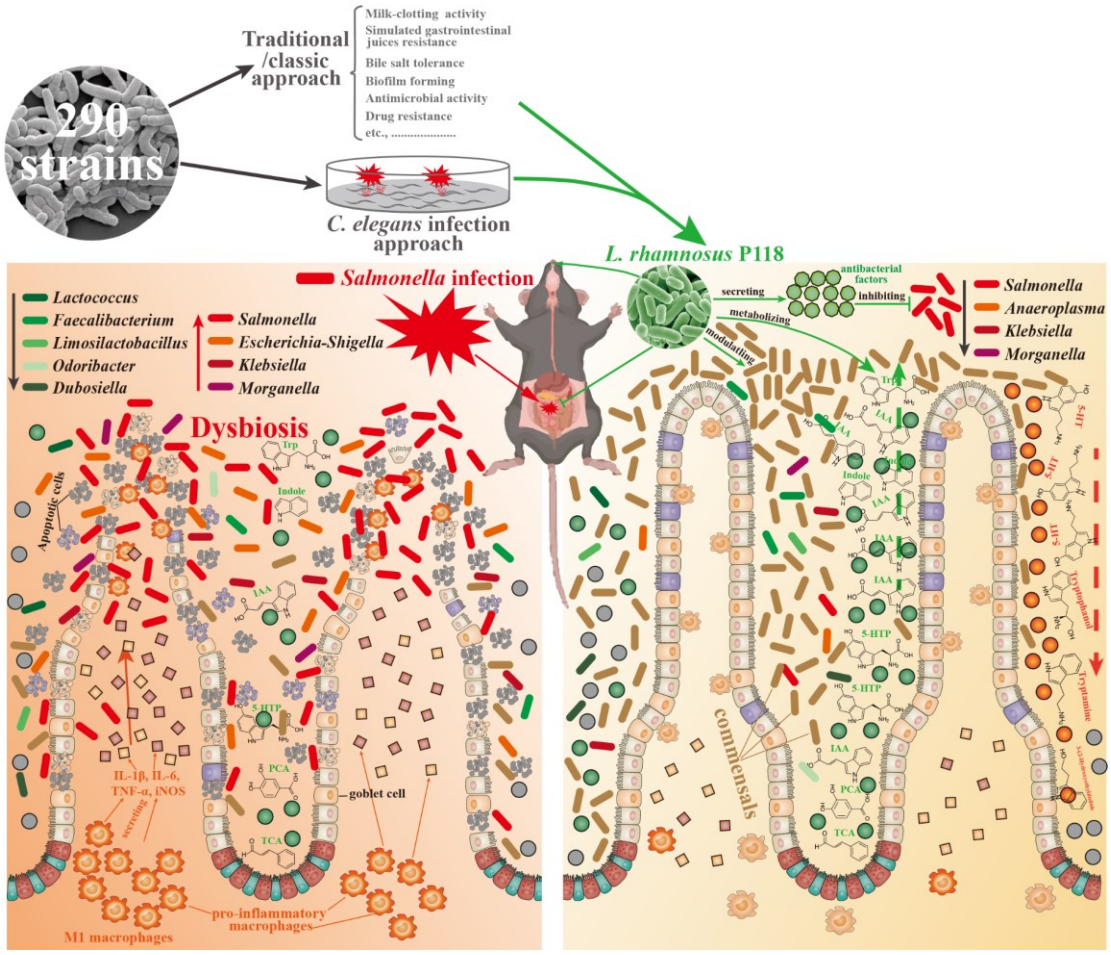

Figure 7. *Lacticaseibacillus rhamnosus* P118 strain with great probiotic properties was screened from 290 purified isolates through two distinctive screen approaches, and

1076 P118 strain was underscored for protective effects on a murine infection model. Further,
1077 multi-omics analysis pinpointed the microbe-derived tryptophan/indole could be the
1078 importance of P118 probiotic properties. Nevertheless, the newly found P118 enhances
1079 host tolerance to *Salmonella* infections via various pathways, including direct
1080 antibacterial actions, inhibiting *Salmonella* colonization and invasion, attenuating pro-
1081 inflammatory responses of intestinal macrophages, and modulating gut microbiota
1082 mediated by microbe-derived indole metabolites.

1083

1084

1085 **Table 1** A list of probiotic isolates recovered from examined samples

Source	Name	Number of isolates
Yogurt	*Streptococcus salivarius ssp. thermophilus*	63
	Lacticaseibacillus paracasei	18
	Lactobacillus acidophilus	17
	Lactobacillus zeae	10
	Lacticaseibacillus rhamnosus	4
	Lacticaseibacillus casei	4
	Lactobacillus delbrueckii	6
piglet intestine	*Limosilactobacillus mucosae*	16
	Lactobacillus johnsonii	38
	Limosilactobacillus reuteri	16
	Limosilactobacillus vaginalis	11
	Lactobacillus crispatus	9
	Lactobacillus salivarius	6
	Lactobacillus amylovorus	3
	Enterococcus faecium	38
	Enterococcus faecalis	31
Total		290

1086 **Supplementary information**

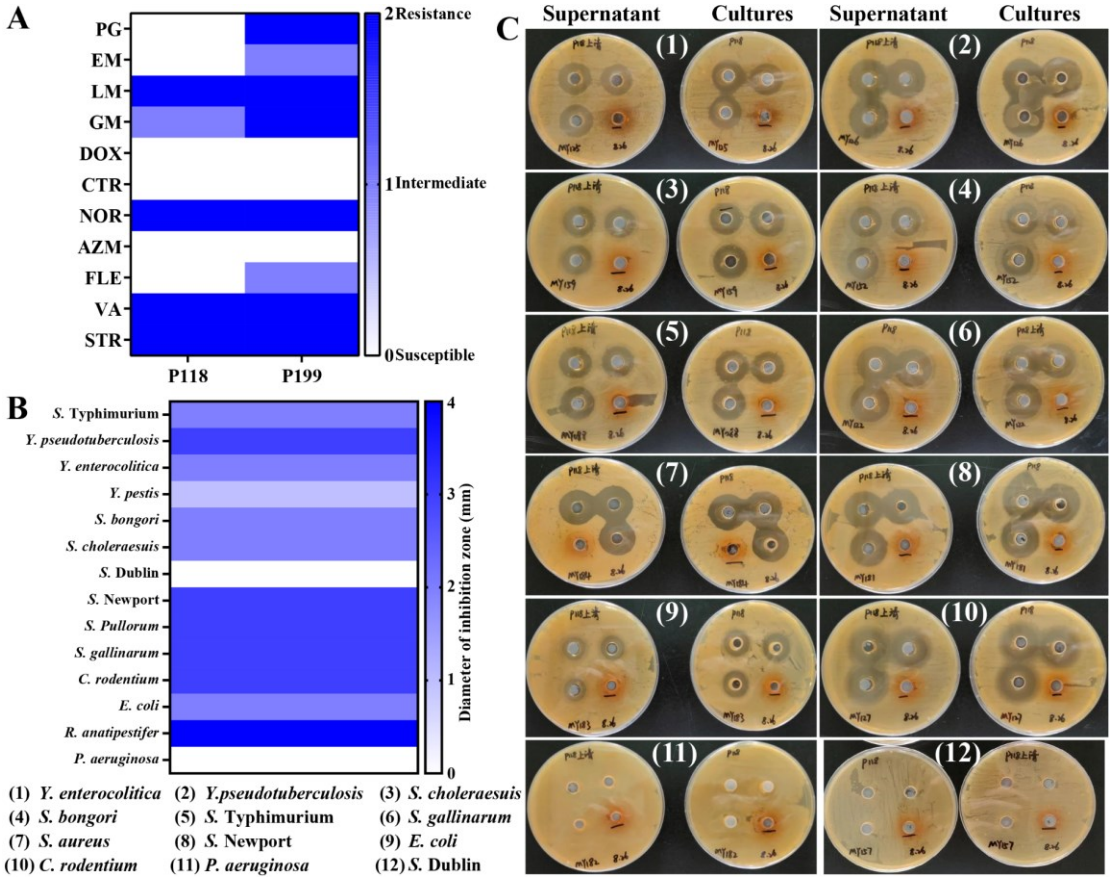

Figure S1 (**A**) Drug resistance candidate probiotic isolates (P118 and P199). (**B, C**) Broad-spectrum antibacterial activities of P118 fermented supernatants and cultures.

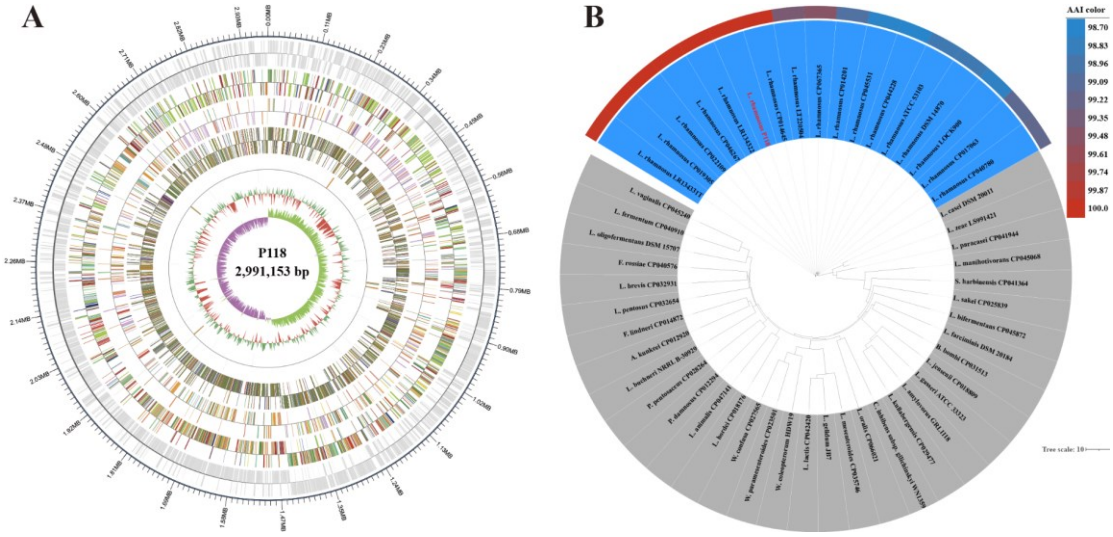

Figure S2. (**A**) Circular genome map of *L. rhamnosus* P118. (**B**) phylogenetic trees of *L. rhamnosus* P118 and nearest phylogenetic neighbors constructed by average amino acid identify (AAI). Color gradients indicate the percentage of conserved average

nucleotide identity (ANI) between each isolate and respective nearest subspecies phylogenetic neighbors.

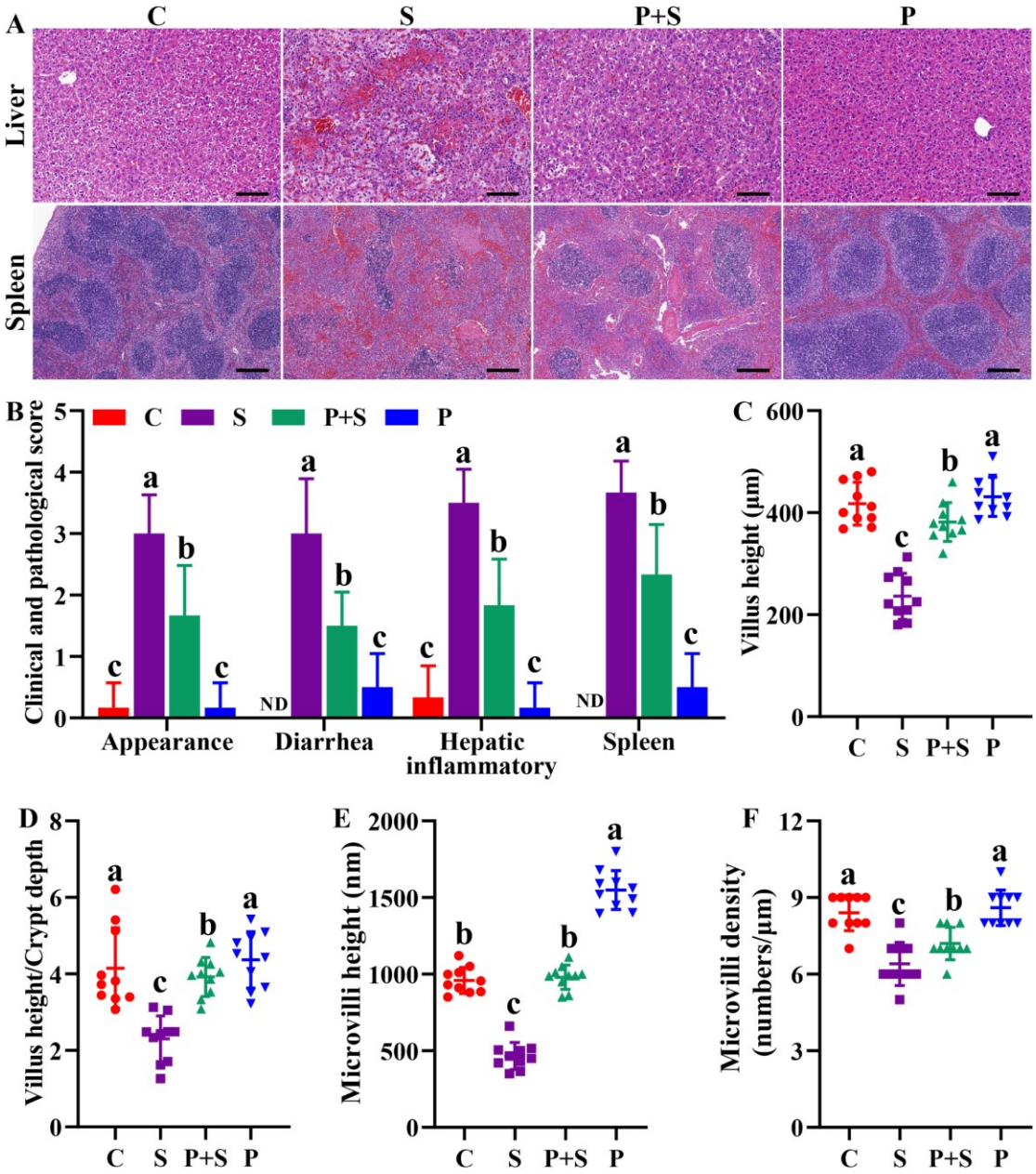

Figure S3. Clinical and Histopathological observation. (**A**) Representative images of H&E staining tissues (liver, spleen). Scale bar with 100 μm. (**B**) Clinical symptom score. Histopathological quantification of H&E staining (**C & D**) and TEM (**E & F**) images observed in the ileum. Different lowercase letters indicate a significant difference ($P < 0.05$). C: PBS group; P: P118 administered group; S: *S*. Typhimurium-infected group;

1102 P+S: P118 protective group.

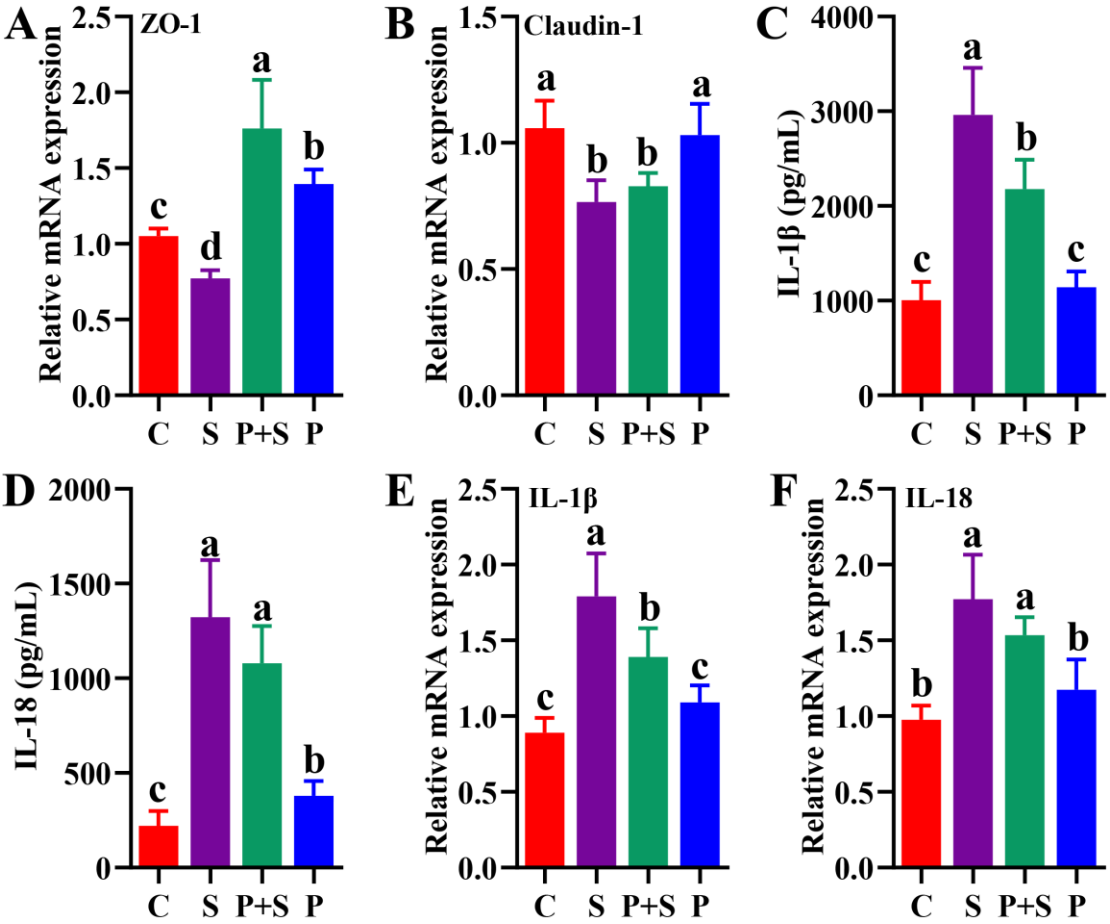

1103

1104 **Figure S4.** Gene and protein expression level of tight junction protein (ZO-1, Claudin-

1105 1) and inflammatory cytokines (IL-1β, IL-18) in ileum and serum of mice. Different

1106 lowercase letters indicate a significant difference ($P < 0.05$). C: PBS group; P: P118

1107 administered group; S: *S*. Typhimurium-infected group; P+S: P118 protective group.

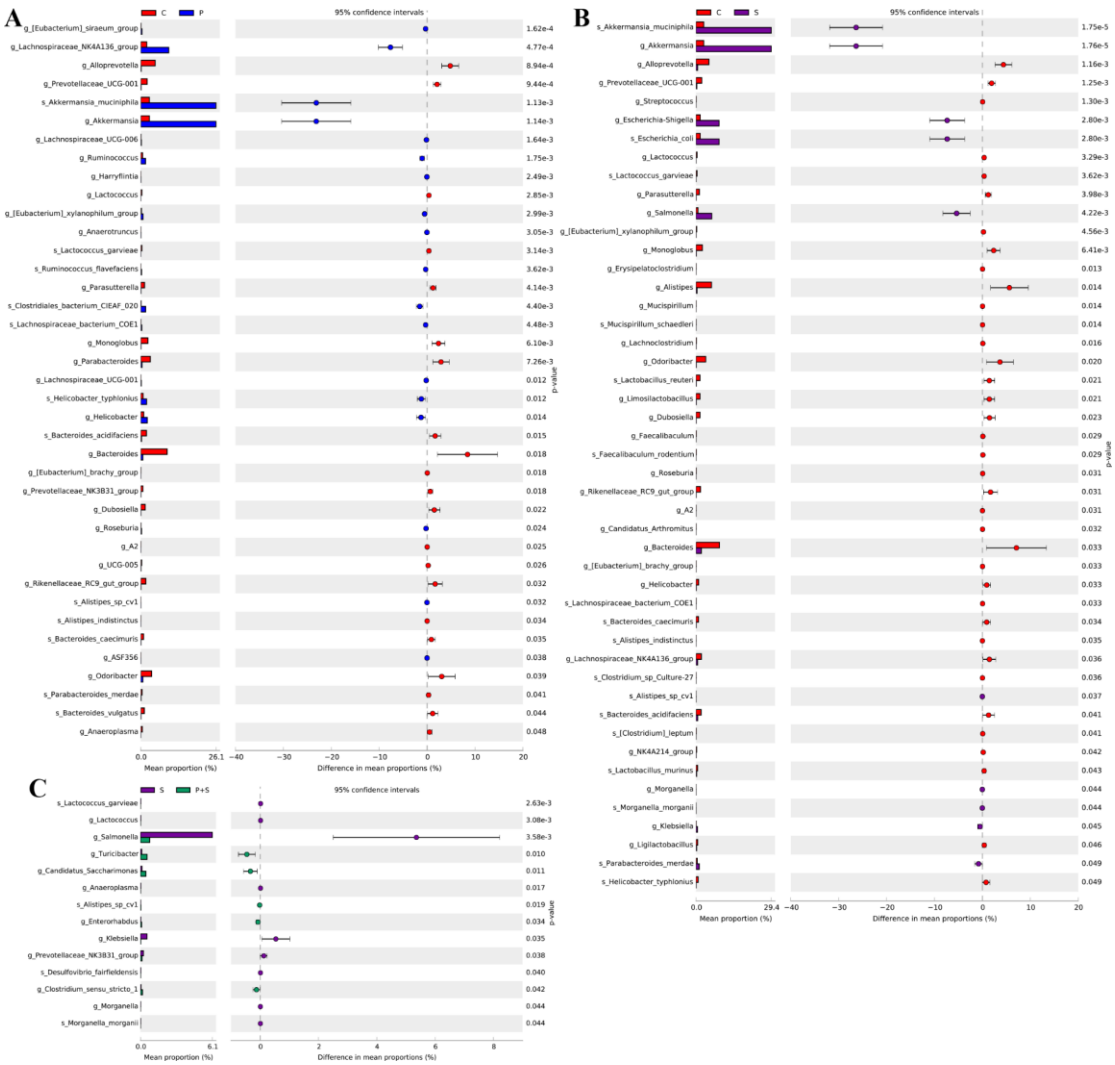

Figure S5. Comparison of intestinal microbes by the analysis of statistical analysis of taxonomic and functional profiles (**STAMP**) software with a two-sided Welch's t-test. (**A**) C *vs* P, (**B**) C *vs* S, (**C**) S *vs* P+S. The prefixes "g_" and "s_" represent the annotated levels of genus and species. C: PBS group; P: P118 administered group; S: *S.* Typhimurium-infected group; P+S: P118 protective group.

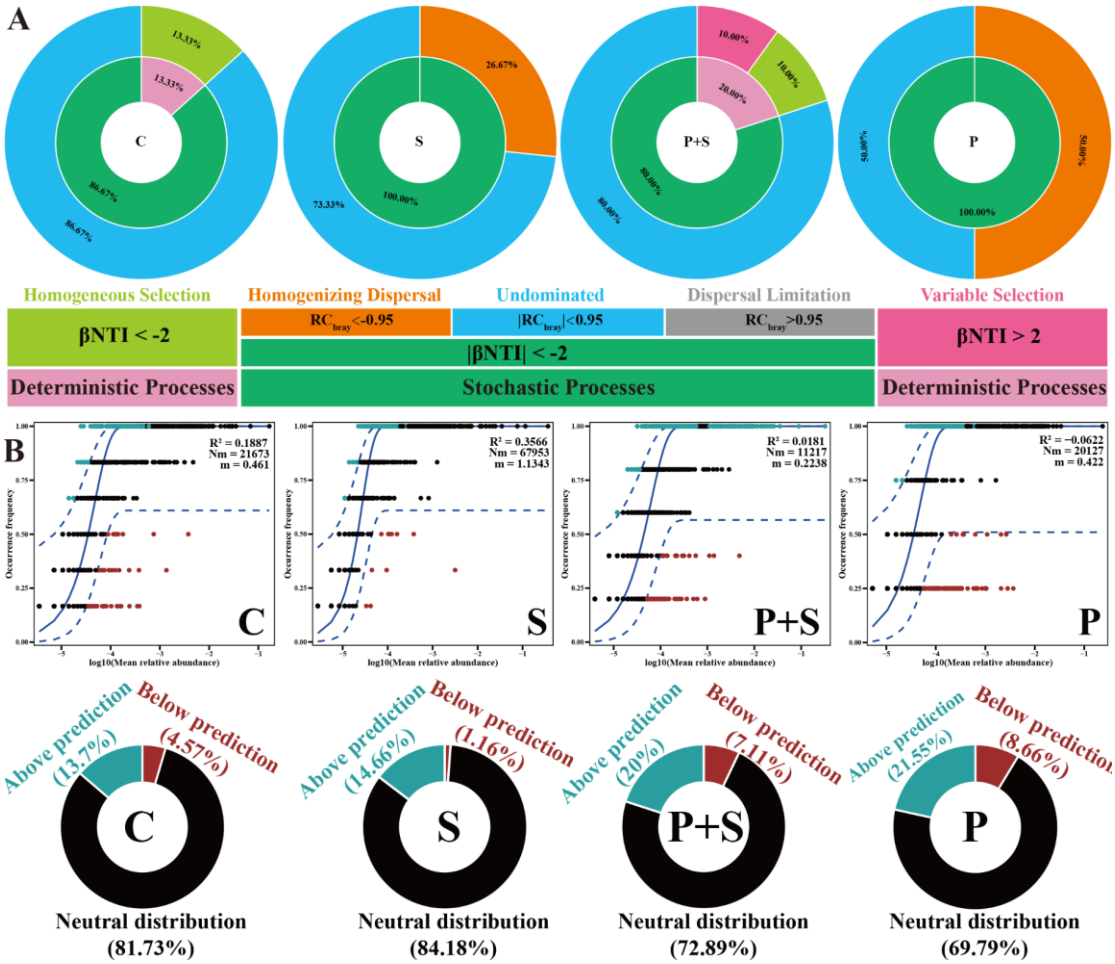

Figure S6. *L. rhamnosus* P118 alters gut microbial community assembly. (**A**) Ecological processes of gut microbes. The inner circle indicates the percentage of deterministic and stochastic assembly processes. The outer circle indicates the contribution of detailed ecological processes. **(B)** The fit of neutral community model (NCM) of community assembly for gut microbes. The best fit to NCM and 95% CIs around the best fit to NCM were indicated by solid and dashed blue lines, respectively. Light blue and dark red dots indicate OTUs that occur more (above prediction) or less (below prediction) frequently than predicted by NCM, respectively, while black dots indicate the OTUs that occur within neutral prediction (neutral distribution). Donut charts shows the distinct fitting proportions of OTUs predicted by NCM. C: PBS group; P: P118 administered group; S: *S.* Typhimurium-infected group; P+S: P118 protective

group.

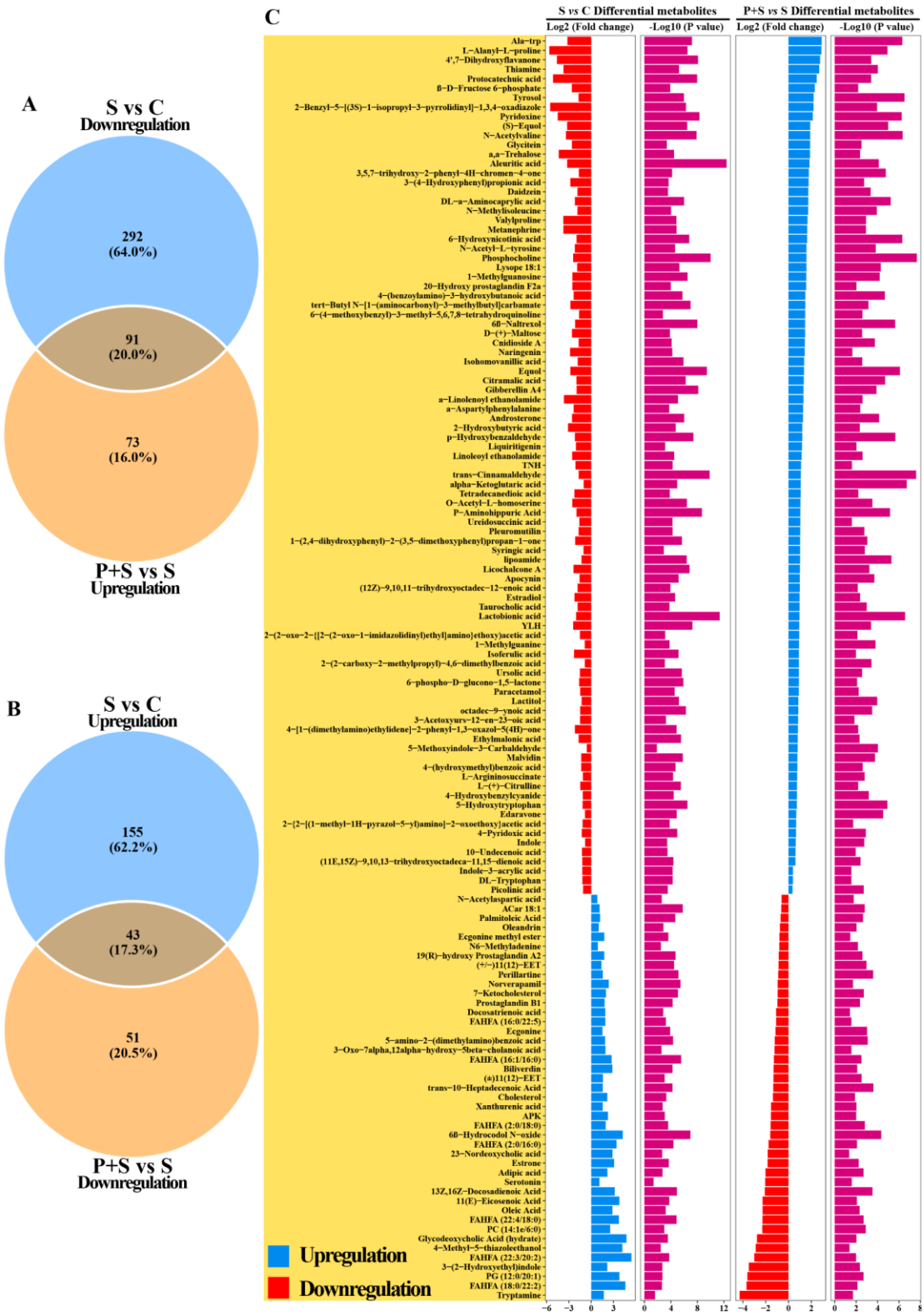

Figure S7. Analysis of differential fecal metabolites. Venn diagram based on

differential fecal metabolites (**A**) down-regulated in "S *vs* C" and up-regulated in "P+S *vs* S", (**B**) up-regulated in "S *vs* C" and down-regulated in "P+S *vs* S". (**C**) Significant differential fecal metabolites in "S *vs* C" and "P+S *vs* S". C: PBS group; P: P118 administered group; S: *S*. Typhimurium-infected group; P+S: P118 protective group.

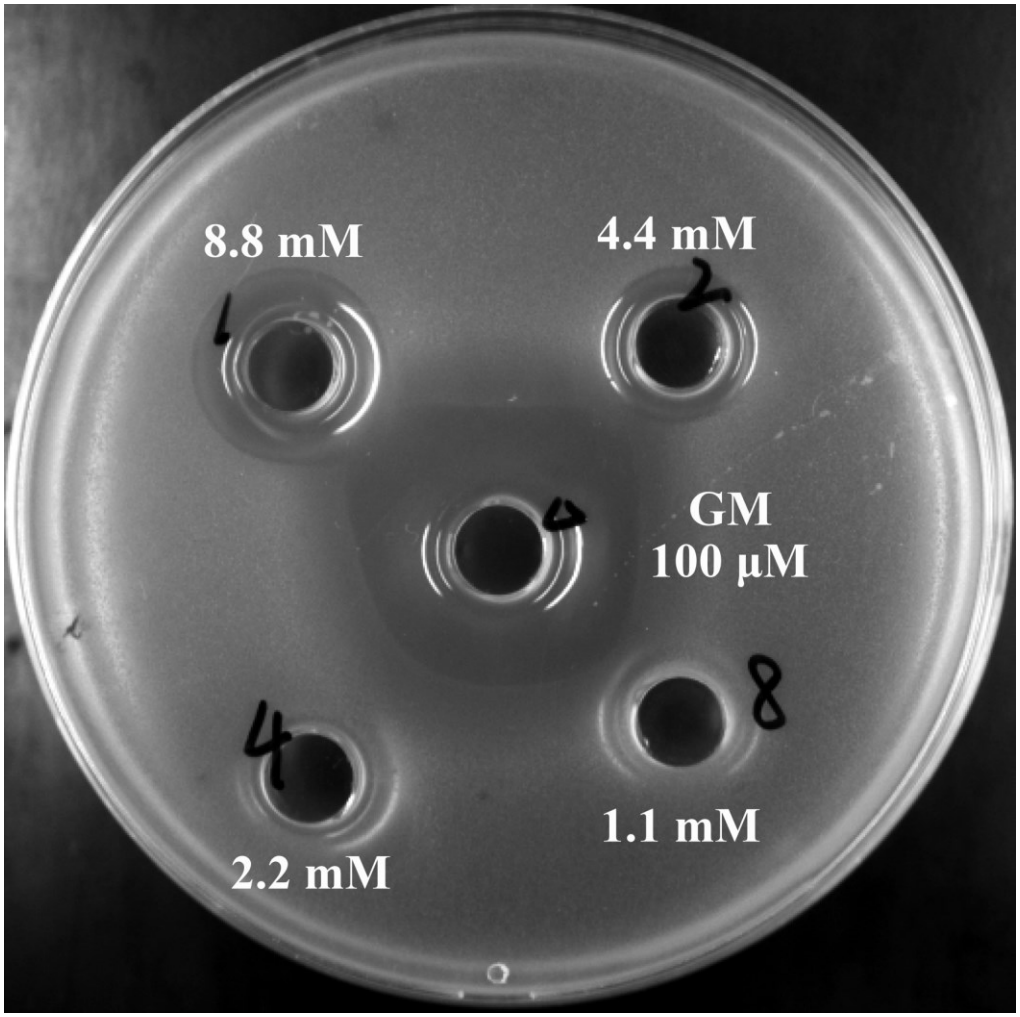

Figure S8. Antibacterial activities of indole-3-acrylic acid. GM: 100 μg/mL gentamicin.

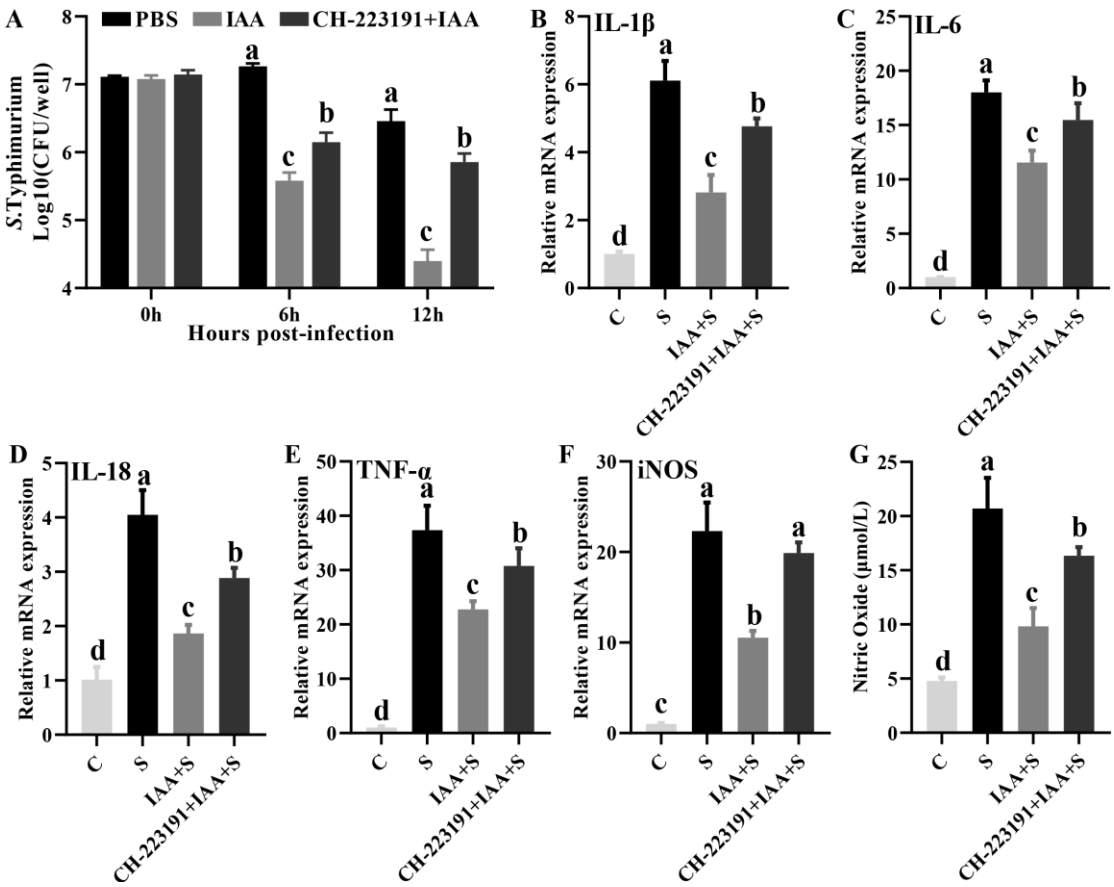

Figure S9. Indole-3-acrylic acid enhances bactericidal capacity and exerts anti-inflammatory activity in RAW 264.7 cells. Different lowercase letters (a, b, c, d) indicate a significant difference ($P < 0.05$). C: PBS group; IAA: indole-3-acrylic acid group; S: *S*. Typhimurium-infected group; CH-223191: AHR inhibitor-treated group.

Table S1 Milk-clotting activity of lactic acid bacteria

Table S2 Significance between life span data was calculated using a Mantel-Cox log-rank test

Table S3 Significance between life span data was calculated using a Mantel-Cox log-rank test

Table S4 Species-level identity of *L. rhamnosus* P118. The draft genome of P118 was queried using the NCBI non-redundant prokaryotic database available through MIGA

1149 (http://www.microbial-genomes.org). P-values reflect confidence in the assignment as
1150 each taxonomic rank.

1151 **Table S5** *L. rhamnosus* P118 draft genome nearest subspecies phylogenetic neighbors.
1152 Average nucleotide identity (ANI) and average amino acid identity (AAI) using both
1153 percent identity and a fraction of genome shared as determined through MIGA
1154 (http://www.microbial-genomes.org) query of the NCBI non-redundant prokaryotic
1155 genomes database were considered for ranking likelihood of nearest subspecies
1156 phylogenetic neighbors for duplicate isolates of each *Lacticaseibacillus* species.

1157 **Table S6** Primers used for the quantitative PCR

1158 **Table S7** The criteria of clinical symptom scores

1159 **Table S8** ANOSIM, PERMANOVA and MRPP analysis of microbial diversity among
1160 treatments

1161 **Table S9** ANOSIM, PERMANOVA and MRPP analysis of fecal metabolites among
1162 groups

1163 **Table S10** Significant differential fecal metabolites in "S *vs* C" and "P+S *vs* S"

1164 **Table S11** Prediction of aminotransferase class and tryptophan binding affinity in *L.*
1165 *rhamnosus* P118

1166 **Table S12** Tryptophan metabolism and indole derivatives in *L. rhamnosus* P118
1167 cultures